Aircraft D-100 Final Design Report

A 201-Passenger, 2,006-Nautical-Mile, Mach 0.75 Narrow-Body Airliner

AME 481 Aircraft Design, Spring 2026

Gabe Kozielec

University of Southern California, Department of Aerospace and Mechanical Engineering

May 8, 2026

Table of Contents

Abstract

Aircraft Overview

1 Introduction

1.1 Top-level mission requirements

1.2 Phase A summary

1.3 Phase B scope and report organization

2 Configuration

3 Fuselage Design

3.1 Cross-section

3.2 Cabin layout (LOPA)

3.3 Cargo

3.4 Cockpit

3.5 Nose contour

3.6 Tailcone contour

3.7 Fuselage proportion

4 Wing Design

4.1 Planform

4.2 Airfoil family

4.3 Spanwise lift distribution and Oswald efficiency

4.4 Tip deflection and structural weight

4.5 Buffet check at cruise

4.6 Dihedral and tip strike clearance

4.7 Wing position

4.8 High-lift system, ailerons, spoilers

4.9 Spanwise panel drag distribution

4.10 Structural box

5 Empennage

5.1 Horizontal stabilizer

5.2 Vertical tail

5.3 Trim verification across the CG envelope

5.4 Empennage structure

6 Landing Gear

6.1 Nose gear

6.2 Main gear

6.3 Longitudinal location and pitch rotation

6.4 Strut length

7 Sub-System Distribution

8 Propulsion

8.1 Turbofan versus turboprop

8.2 Engine placement

8.3 Fan diameter, thrust, and engine cycle

9 Mission Performance

9.1 Weight breakdown and CG envelope

9.2 Cost breakdown

9.3 Cruise drag breakdown

9.4 Cruise Mach selection

9.5 Cruise altitude

9.6 Cruise CL and L over D against Mach

9.7 Fuel breakdown by mission segment

9.8 Field performance

9.9 Breguet range comparison

9.10 DOC minimization

9.11 Takeoff and landing CL with high-lift devices

9.12 Laminar flow trade

9.13 Three-view and isometric drawings

9.14 Phase A versus Phase B comparison

10 Design Space Studies

10.1 Payload-range

10.2 Fan diameter, with environmental tax

10.3 Specific range against cruise Mach

10.4 Materials trade

10.5 Initial cruise altitude at 25,000 ft

10.6 Liquid hydrogen against Jet-A

10.7 Battery-electric range

10.8 +20 percent design range

10.9 Code C span

11 Summary and Conclusions

11.1 Phase B convergence

11.2 Phase A versus Phase B reconciliation

11.3 What the design space studied

11.4 Limitations

11.5 Recommendations for Phase C

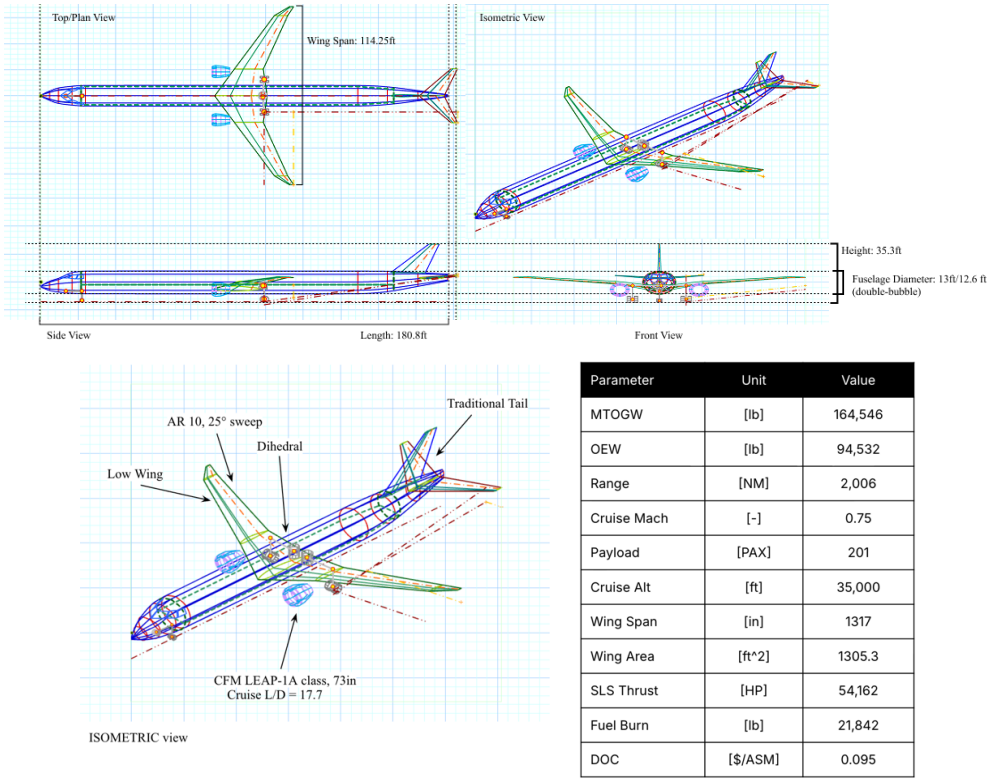
12 AI Use Discussion

References

Abstract

Aircraft D is a Phase B conceptual design for a single-aisle, 201-passenger narrow-body airliner sized to a 2,006-nautical-mile mission at Mach 0.75 cruise and a 35,000-ft initial cruise altitude. The configuration is a low-wing, twin-turbofan transport with a conventional empennage, two underwing CFM LEAP-1A class engines (73-in fan), a 113.25-ft composite wing of aspect ratio 10 with 25 deg quarter-chord sweep, and a 180.8-ft double-bubble fuselage. Phase B drove the design through the JetSizer-II Mission Sizer to a converged maximum takeoff gross weight of 160,981 lb, an operating empty weight of 92,242 lb, a mission fuel burn of 20,731 lb, a cruise lift-to-drag ratio of 17.7, a balanced takeoff field length of 6,500 ft, and an approach speed of 135 kt at maximum landing weight. The direct operating cost of $0.0940 per available seat-mile is competitive with current narrow-body benchmarks. The Phase B effort produced a Layout of Passenger Accommodations sized for 36 business and 165 economy seats, a wing planform with a three-panel trapezoidal layout and a NASA SC(2) supercritical airfoil family, an empennage sized to a horizontal tail volume coefficient of 1.11 and a vertical tail volume of 0.09, a tricycle landing gear with a four-wheel main bogey, and a propulsion installation tuned by a fan-diameter trade. A nine-case design space study examined payload-range performance, fan diameter with and without an environmental fuel tax, specific range against cruise Mach, structural materials class, initial cruise altitude, mission range stretch, ICAO Code C span, liquid hydrogen substitution, battery-electric substitution, and laminar flow. The studies isolate fan diameter, materials class, and aspect ratio as the strongest cost levers and confirm that hydrogen and battery-electric energy carriers remain infeasible at this airframe and mission. The report closes with a comparison of Phase A targets to Phase B converged values, recommendations for a Phase C iteration, and a discussion of how artificial intelligence tools were used in preparing the report.

Aircraft Overview



Parameter	Unit	Value
MTOGW	[lb]	164,546
OEW	[lb]	94,532
Range	[NM]	2,006
Cruise Mach	[-]	0.75
Payload	[PAX]	201
Cruise Alt	[ft]	35,000
Wing Span	[in]	1317
Wing Area	[ft^2]	1305.3
SLS Thrust	[HP]	54,162
Fuel Burn	[lb]	21,842
DOC	[$/ASM]	0.095

Figure 1. Aircraft D three-view, isometric, and walkaround parameter summary.

1 Introduction

The AME 481 design project for Spring 2026 specifies three top-level missions. Aircraft D is the 201-passenger, 2,006-nmi, Mach 0.75 narrow-body. The airplane must operate from 6,500-ft balanced runways, approach at no more than 145 kt, climb to an initial cruise altitude no lower than 21,000 ft, and meet 14 CFR Part 25 transport-category airworthiness standards [8]. Phase A produced a top-level constraint-diagram sizing and a set of target parameters. Phase B refines that sizing into a complete conceptual design, exercises the design space, and documents every input, constraint, and result.

1.1 Top-level mission requirements

The mission profile, payload, and environmental performance targets are summarized in Table 1. All values are taken from the project statement of work [13] and from the project kickoff document [15].

Table 1. Top-level mission requirements for Aircraft D.

Parameter	Value	Source
Passengers	201	Mission requirements
Range	2,006 nmi	Mission requirements
Cruise Mach	0.75	Mission requirements
Initial cruise altitude	21,000 ft minimum	Performance requirements
Takeoff field length	6,500 ft balanced	Performance requirements
Approach speed at MLW	145 kt maximum	Performance requirements
Aircraft length	74 m maximum	Cabin requirements
Cargo allowance	7 ft^3 per passenger	Cabin requirements
Pitch rotation angle	10 deg minimum	Landing gear requirements
Maneuvering load factor	2.5 g limit	Performance requirements
Minimum static margin	10 percent MAC	Performance requirements
Fuel	Jet-A baseline	Cost model requirements

Two requirements bind the configuration directly. The 145-kt approach speed sets a wing-area floor through landing CL_{max}, and the 6,500-ft balanced field length sets the engine sea-level static thrust and the high-lift system together. Every other top-level number is comfortably interior to its constraint band.

1.2 Phase A summary

Phase A sized the airplane on the JetSizer constraint diagram and set initial cycle and weight targets. Table 2 lists the Phase A parameters that bounded the Phase B effort against the Phase B converged values.

Table 2. Phase A targets compared to the Phase B converged design.

Parameter	Unit	Phase A	Phase B
MTOGW	lb	109,817	160,981
Empty weight fraction	-	0.504	0.573
Cruise L/D	-	18.7	17.7
Propulsive efficiency	-	0.42	0.38
Cruise Mach	-	0.75	0.75
Cruise altitude	ft	35,000	35,000

Parameter	Unit	Phase A	Phase B
Mission fuel burn	lb	not set	20,731
DOC	$ per ASM	not set	0.0940

Phase B is heavier than Phase A by about 47 percent on MTOGW and 14 percent on empty weight fraction. The growth is dominated by the long, slender fuselage that emerged from a detailed cabin layout, and by the cabin-systems weight (galleys, lavatories, accessibility provisions, seats) that Phase A could only treat as a fixed-equipment lump sum. Cruise L/D is 5 percent below the Phase A target because the wing was sized by the approach-speed constraint rather than by L/D-max, and propulsive efficiency dropped 9 percent because the fan diameter converged to 73 in rather than the larger value Phase A had assumed. The cruise Mach and altitude held to their Phase A values, both of which proved near-optimal in Phase B trade studies.

1.3 Phase B scope and report organization

The Phase B effort covers fuselage layout (section 3), wing design (section 4), empennage sizing (section 5), landing gear (section 6), sub-system distribution (section 7), propulsion (section 8), mission performance (section 9), and a nine-case design space study (section 10). Section 11 closes with a Phase A versus Phase B reconciliation, limitations, and recommendations. Section 12 documents how AI tools were used. All numerical results trace back to the converged JetSizer-II workbook column for Aircraft D unless explicitly noted otherwise. Cross-references between sections cite section numbers rather than file or sheet names.

2 Configuration

The configuration was settled before the Phase B sizing loop opened, on the strength of mission similarity to in-service single-aisle narrow-bodies. Aircraft D is a low-wing, single-aisle, twin-turbofan transport with two underwing engines, a conventional empennage with a low-set horizontal stabilizer and a single vertical fin, a tricycle landing gear with a four-wheel main bogey, and a double-bubble fuselage cross-section sized for 6-abreast economy seating.

This anchors the design close to the established narrow-body cluster of the 737 MAX, A320neo, A220-300, and 757-200 [1] [2], where field length, approach speed, gear length, sub-system architectures, and certification credit are well understood. Anchoring the configuration limits Phase B's risk on parameters that are not the focus of the design, and lets the design space study isolate the levers that actually move cost and fuel burn (fan diameter, structural materials, span limits, and laminar flow) rather than spend points on configuration-level uncertainty.

The four configuration choices that mattered, and the reasoning that drove them, are:

1. Low wing rather than high wing. Low wing simplifies main-gear retraction into the wing-fuselage junction, keeps the cargo deck at belt-loader height, and reduces the engine-out yaw moment because pylon-mounted engines sit closer to the airplane centerline. Every current production narrow-body uses a low wing for these reasons [1].

2. Underwing pylon-mounted engines rather than aft-fuselage mount. Underwing pylons relieve wing bending with engine weight, keep cabin noise low, and allow ground-level engine maintenance access. Aft-mounted engines simplify high-lift device design because the wing trailing edge is unobstructed, but they raise empty weight, complicate the cabin floor, and are not the dominant choice for a 200-class narrow-body.
3. Conventional empennage rather than T-tail. A low-set horizontal stabilizer attaches directly to fuselage frames, removes the deep-stall risk that T-tails carry at high angle of attack, and frees the aft fuselage volume that a T-tail's vertical-tail spar carry-through would otherwise consume. The aft fuselage volume is needed for the long aft cabin that the 18 percent business-class allocation produces.
4. Double-bubble fuselage rather than single circular section. The double-bubble (upper lobe 156 in, lower lobe 151 in, lower-lobe centroid 10 in below the upper) gives 6-abreast economy seating across a 148-in interior cabin width and a cargo bay below the cabin floor sized for one LD3-45 container per station. A single circular section sized to the same interior width would force the cargo floor lower and add wetted area without commensurate volume.

The configuration was carried unchanged from Phase A into the Phase B sizing loop. No configuration variable was reopened during the design space study.

3 Fuselage Design

The fuselage is sized by the cabin and cargo it has to carry. Phase B started from the project's two-class seating requirement and the per-passenger cargo volume, derived a Layout of Passenger Accommodations, and built up the cross-section, cockpit, nose, and tailcone from there. Total fuselage length converged at 2,170 in (180.8 ft, 55.10 m), well below the 74-m project ceiling.

3.1 Cross-section

The fuselage is a double-bubble of the form used on every modern narrow-body. The upper lobe carries the cabin, the lower lobe carries cargo and systems, and the two lobes share a structural floor at the cabin level. Table 3 lists the cross-section parameters and the constraints they had to clear.

Table 3. Fuselage cross-section parameters.

Parameter	Value	Driver
Upper lobe diameter	156 in	6-abreast economy at 18-in seat pan and 2-in armrest
Lower lobe diameter	151 in	LD3-45 container fit at converged cargo-floor depth
Lower lobe vertical offset	10 in below upper lobe centroid	Cargo-floor depth at Z = -74 in

Parameter	Value	Driver
Frame thickness	4 in each lobe	Standard transport-class structural reserve
Cabin floor	Z = -21 in	Above the lobe intersection, below the headroom envelope
Interior cabin width	148 in	156 in upper lobe minus 2 times 4-in frame
Cargo-floor lateral width	80.1 in	Single LD3-45 fit, 60.4 in container plus 19.7 in service walkway

The 148-in interior cabin width is the single most constraining cross-section number. It accepts a 3-plus-3 economy layout exactly, with no spare width. Any future widening of the seat pan or the armrest would break the layout. Above the seat zone, the cross-section provides standard transport headroom and overhead bin volume sized for one carry-on roll-on per passenger.

3.2 Cabin layout (LOPA)

Aircraft D carries 36 business-class seats and 165 economy seats, of which 3 are dedicated special-mobility positions. Both class counts are clean row-multiples in the converged layout, which avoids partial-row geometry and lets each zone carry a recognizable function. The full cabin layout is shown in Figure 2.

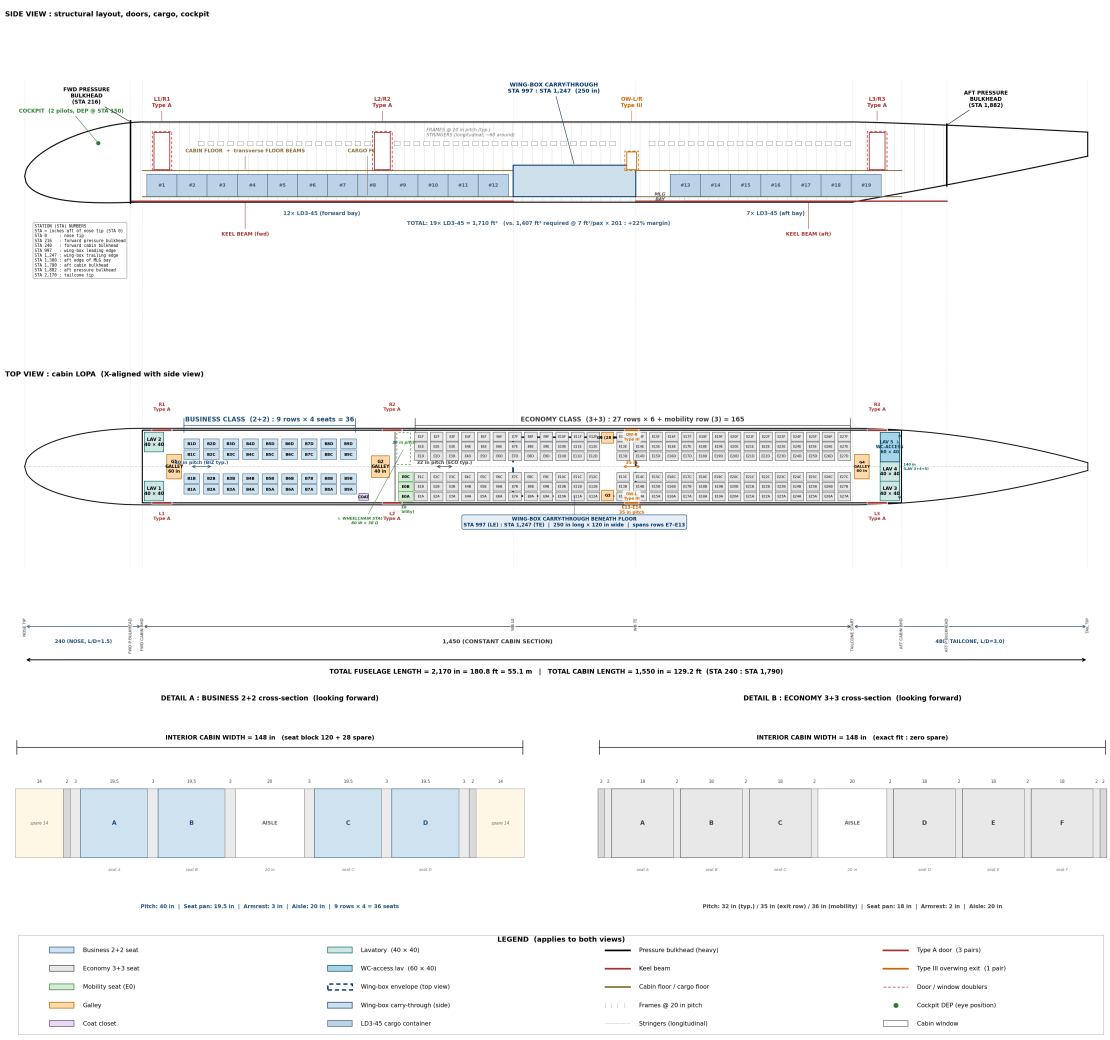


Figure 2. Layout of Passenger Accommodations for Aircraft D, showing forward and aft service zones, business-class cabin, special-mobility row, economy cabin, and cargo bay.

Table 4 lists the seating breakdown and the project-spec compliance check.

Table 4. Aircraft D seating summary.

Item	Value	Project requirement
Business class seats	36 (9 rows of 2 plus 2)	15 percent minimum (= 31 seats)
Special mobility seats	3 (left side, row E0)	1 percent minimum (= 3 seats)
Economy class seats	162 (27 rows of 3 plus 3)	balance of 201
Total seats	201	201
Business class fraction	17.9 percent	15 percent minimum

Item	Value	Project requirement
Special mobility fraction	1.49 percent	1 percent minimum
Lavatories	5, including 1 wheelchair-accessible	At least 1 wheelchair-accessible
Galleys	4 (forward, class transition, mid-economy, aft)	not specified
FAA cabin attendants	5	one per 50 passengers

Three configuration choices set the row counts. The business-class allocation was set at 36 seats because it divides cleanly into 9 rows of 2-plus-2 at 40-in pitch, leaves 162 seats divisible into 27 rows of 3-plus-3 economy at 32-in pitch, and gives a 17.9 percent business fraction comfortably above the 15 percent minimum. Going to 31 seats (the floor) would force a partial row of business class and break the row math on the economy side. Going to 40 seats would leave 161 economy seats, also not a whole number of rows. The 36-seat configuration is the cleanest layout that meets the spec.

The special-mobility row sits immediately aft of the L2 class-transition vestibule, on the left side only, with three seats featuring removable aisle-side armrests, wheelchair-anchor floor studs, and 36-in pitch. The right side of the same row is open floor for wheelchair staging and ambulatory passenger transfer. Placement aft of the class-transition door gives the shortest path to a Type A exit, and the flat floor at this station avoids the wing-box crown that runs from row E13 through E14.

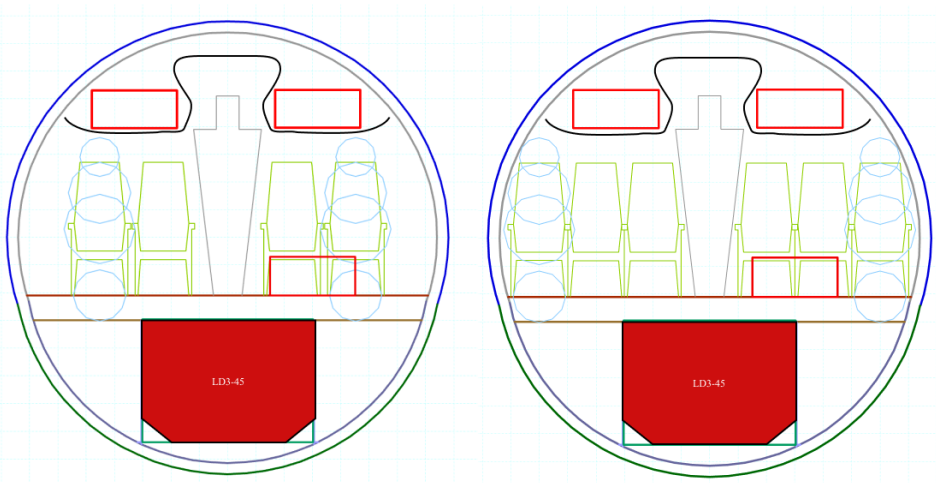


Figure 3. Business class 2-plus-2 and economy 3-plus-3 seating geometry across the 148-in interior cabin width.

Cabin layout zones run from forward to aft as listed in Table 5. The cumulative cabin length is 1,550 in (129.2 ft).

Table 5. Cabin zone-by-zone length.

Zone	Length (in)	Cumulative (in)
Forward L1 vestibule, G1 galley, two lavatories	80	80
Business class, 9 rows at 40-in pitch	360	440
Coat closet	24	464
Class transition L2 vestibule, divider, G2 galley	52	516
Special mobility row E0	36	552
Economy E1 to E12, 12 rows at 32-in pitch	384	936
Mid-cabin G3 service	28	964
Overwing exit rows E13 and E14, 2 rows at 35-in pitch	70	1,034
Economy E15 to E27, 13 rows at 32-in pitch	416	1,450
Aft L3 vestibule, G4 galley, three lavatories	100	1,550

Exit configuration follows 14 CFR Part 25.807. Three Type A exit pairs (L1/R1, L2/R2, L3/R3) are placed at the forward, class-transition, and aft zones. Two Type III overwing exits sit at rows E13 and E14, in the only span where the L2 to L3 separation would otherwise exceed the 60-ft maximum allowable inter-exit spacing. The Type III rows carry 35-in pitch rather than the standard 32-in to satisfy adjacent-row requirements.

Five lavatories serve the 201-passenger cabin at a ratio of 40.2 passengers per lavatory, on industry practice for transport-class aircraft [1]. The wheelchair-accessible lavatory is in the aft block adjacent to the standard lavatories and meets accessibility-guidance turning radius and grab-bar requirements. Four galleys are distributed by service load, with the two large units fore and aft, a service galley at the class transition, and a small cart bay at the mid-economy break to reduce aft-galley congestion on longer turns.

3.3 Cargo

Cargo is carried below the cabin floor in single-row LD3-45 containers. The lateral width of the cargo bay at the converged cargo-floor depth is 80.1 in, which fits one 60.4-in-wide LD3-45 per station and leaves 19.7 in for service walkway, conduit routing, and structural framing. A two-abreast layout would need

120.8 in and is not available without raising the cargo floor several inches. Figure 4 shows the container fit at the cargo-floor station.

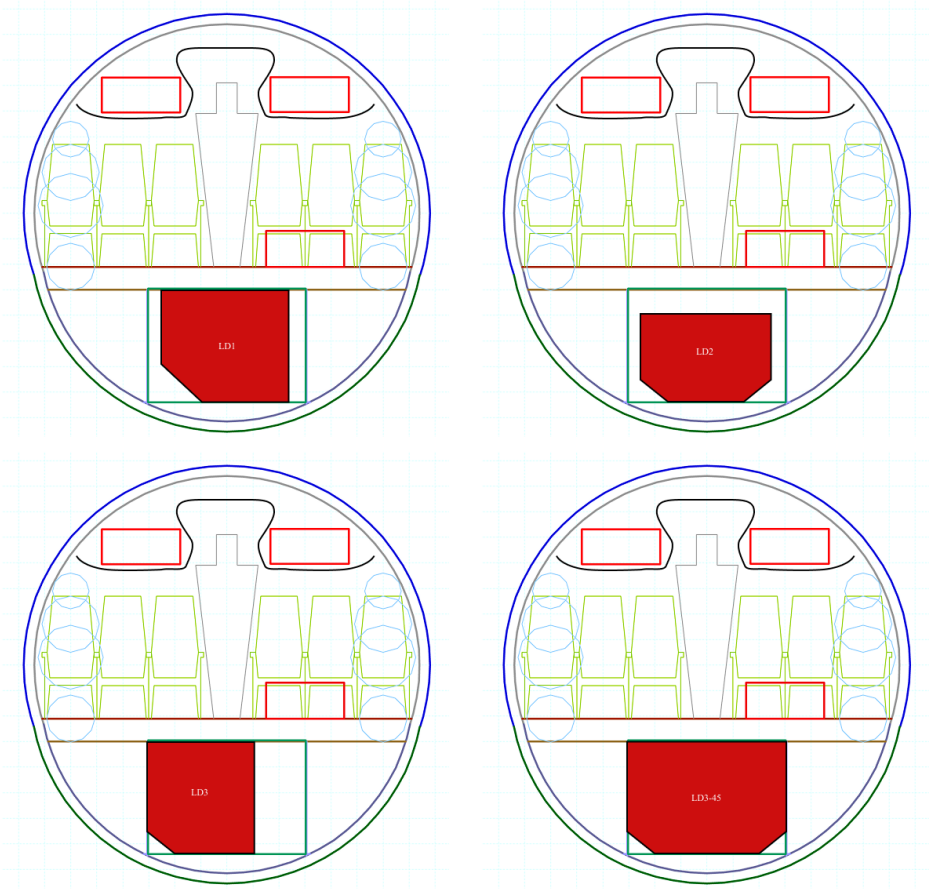


Figure 4. LD3-45 container fit at the Aircraft D cargo-floor station, showing single-row stowage and service walkway.

The available cargo bay length is 1,200 in (100 ft), after subtracting 250 in for the wing-box carry-through and 100 in for the main landing-gear bay from the 1,550-in cabin length. Nineteen LD3-45 stations fit in that length at the 61.5-in container length, for an installed capacity of 1,710 ft^3. The project requirement of 7 ft^3 per passenger is 1,407 ft^3, so the converged design carries 303 ft^3 of margin over the spec floor with all 19 stations loaded. The minimum mission load is 16 LD3-45 containers in 984 in (82 ft) of bay length.

3.4 Cockpit

The cockpit follows transport-category practice for a 201-passenger, 2,006-nmi narrow-body. Crew is two pilots, captain and first officer, with a jumpseat for an FAA observer or relief crew. No flight engineer is required given a 2040-entry-into-service glass-cockpit avionics suite. The 5-attendant cabin crew is set by the FAA one-per-50-passenger rule and is independent of the flight crew complement.

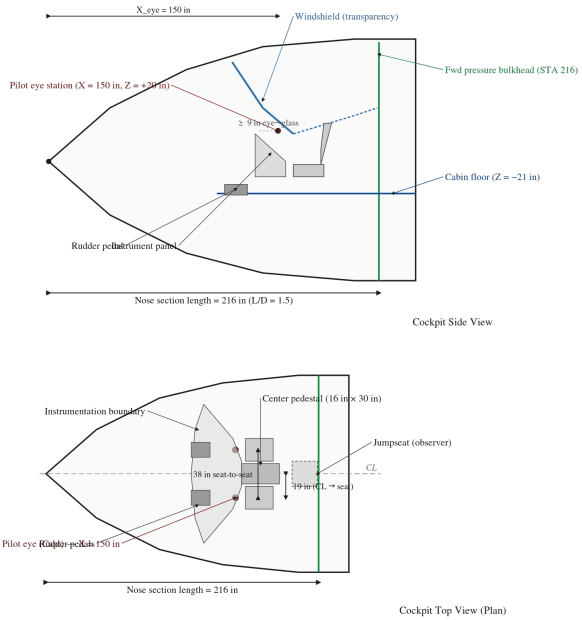


Figure 5. Cockpit layout showing pilot stations, center pedestal, design eye position, and cabin door.

Table 6 lists the geometric parameters of the cockpit. Pilot eye stations sit 19 in from the fuselage centerline, inside the 18 to 20 in band specified in the design requirements (cockpit appendix), and 10 in aft of the windshield transparency, 1 in inside the 9-in minimum. The center pedestal between the seats is 16 in wide and houses the throttle quadrant, the FMS control display units, and the trim wheel.

Table 6. Cockpit geometric parameters.

Parameter	Value	Driver
Crew	2 pilots, 1 jumpseat	FAR Part 121, 2040 EIS avionics
Pilot lateral offset from centerline	19 in	Appendix A.4: 18 to 20 in band
Pilot eye to transparency	10 in	Appendix A.4: 9 in minimum
Design eye station, X from nose tip	150 in	Transport practice for over-nose vision
Design eye height above cabin floor	12 in	Adjustable seat plus standard cushion height
Center pedestal width	16 in	Industry-standard throttle and FMS clearance
Cockpit pressure bulkhead	216 in from nose tip	90 percent of nose length per Plot S75

Parameter	Value	Driver
Cabin door	240 in from nose tip	At cockpit-cabin section transition

Pilot down-vision angle for approach is set by the eye position relative to the drooped nose tip. With 0.2-heights nose droop (32 in below the centerline) over the 240-in nose length, the geometric over-nose angle from the design eye position to the nose tip is about 12 deg. Combined with the 3-deg approach path, this gives an effective approach-flare vision envelope adequate for visual approaches at the runway threshold without forcing the pilot to lean forward against the harness.

3.5 Nose contour

The nose contour is fixed by three JetSizer parameters: a 1.5 fineness ratio (length over diameter), 0.2-heights tip droop, and a forward-pressure-bulkhead station at 90 percent of the nose length. Figure 6 shows the resulting contour.

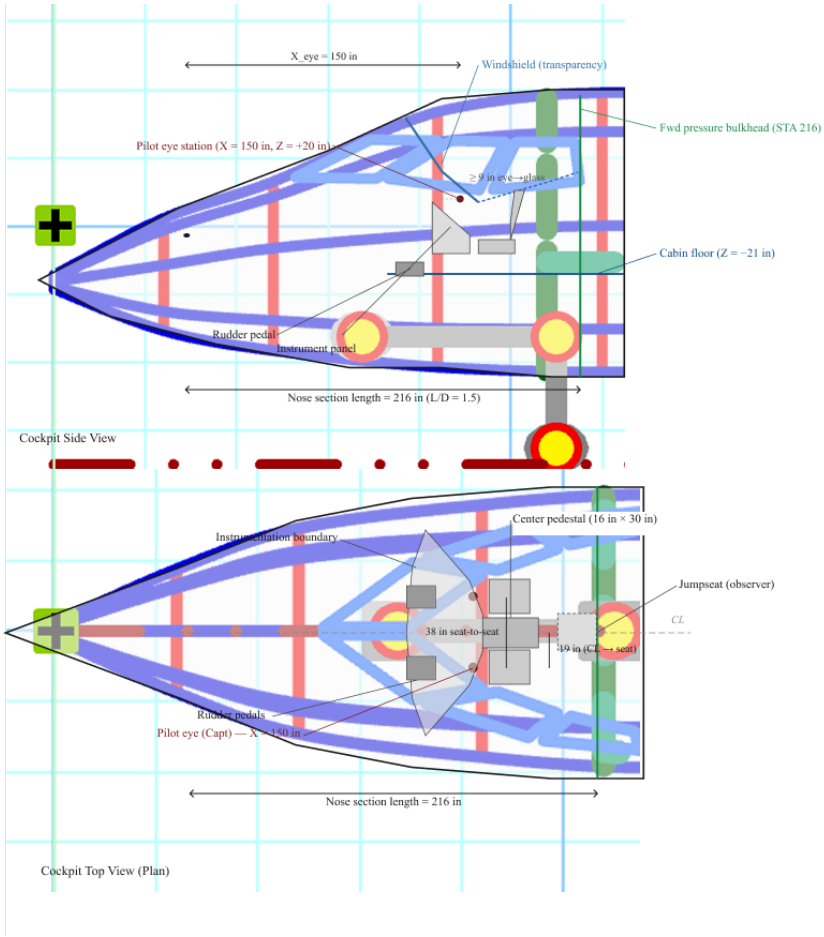


Figure 6. Nose contour profile and three-view, showing 240-in length, 0.2-heights tip droop, and forward pressure bulkhead at 216 in.

The 1.5 fineness ratio sits in the middle of current transport practice (1.4 to 1.6) and was chosen for three coupled reasons. First, at Mach 0.75 cruise the local Mach number on the nose surface stays well below unity even at 1.5 fineness, so a longer (more slender) nose would not buy any compressibility-drag benefit. Second, the 240-in nose accommodates the radome (forward 60 in for the weather radar), the avionics bay (60 in), the nose landing-gear well (80 in below the cockpit floor), and the unpressurized 40 in of cockpit shell aft of the NLG well to the pressure bulkhead. A shorter nose would force the NLG aft into the cabin or shorten the radome. Third, the 1.5 fineness places the design eye at X = 150 in, the standard transport-category eye station that gives over-nose vision without exotic windshield geometry.

The 0.2-heights tip droop achieves two ends. Over-nose vision during approach increases from an estimated 5 deg with a straight-axis nose to 12 deg with a 32-in droop, comfortably encompassing a 3-deg approach plus the flare. Aerodynamic alignment in cruise also improves slightly: at the cruise CL, the fuselage flies at about 2 deg angle of attack, and a drooped nose presents a more axial profile to the airflow at that angle than a straight-axis nose would.

3.6 Tailcone contour

The tailcone is set by a 3.0 fineness ratio, a 0.2-heights tail-tip rise, lateral and vertical tip taper fractions of 0.1 and 0.3, and an aft-pressure-bulkhead station at 40 percent of the tailcone length. The resulting tailcone is 480 in long, with a tip that is narrow (16 in lateral) and tall (49 in vertical), placing the aft pressure bulkhead 192 in into the tailcone.

The 3.0 fineness ratio sits at the knee of the pressure-drag-versus-length curve for transport tailcones. Increasing fineness from 2.0 to 3.0 captures most of the available pressure-drag benefit; pushing further to 4.0 or 5.0 adds wetted area for diminishing returns. Empirical narrow-body tailcone fineness ratios cluster between 2.8 and 3.1 [1] [6]. The 480-in length also sets the tail moment arm, which in turn lets the converged horizontal-tail volume coefficient sit at 1.11 with a 238-ft^2 tail rather than a larger area.

The 0.2-heights tip rise gives tail-strike clearance during rotation. Without the rise, a 12-deg pitch rotation with main-gear contact 970 in forward of the tail tip would drop the tip 206 in below its static position and drive it into the runway. The 32-in built-in rise recovers about 32 in of tail-strike margin, with additional clearance gained by the horizontal-stabilizer leading edge sitting forward of the tail tip. The asymmetric tip taper (faster lateral than vertical) accommodates the APU exhaust nozzle and the vertical-tail attachment fittings without wasting volume, which is why every commercial transport tailcone has the same characteristic narrow-tall silhouette.

The 40 percent aft-pressure-bulkhead station puts the bulkhead at 1,882 in from the nose tip, leaving 288 in of unpressurized aft tailcone for the APU, APU air inlet, APU exhaust, and the hydraulic and pneumatic runs to the empennage. An earlier bulkhead (lighter, smaller diameter) would shorten the pressurized aft volume; a later bulkhead (heavier dome, larger pressure load) would push the APU and hydraulic runs aft against the tail tip. The 40 percent station is the converged operating point.

3.7 Fuselage proportion

Aircraft D's fuselage-to-wingspan ratio is 1.60 (180.8 ft fuselage over 113.25 ft span). This is higher than any current production narrow-body and warrants explicit justification.

Three drivers produce the proportion. The 18 percent business-class allocation pushes cabin length up: 36 seats at 40-in pitch is 360 in (30 ft) of cabin, or 16.6 percent of the total fuselage length, used by business class alone. The project floor is 15 percent; the cleanest row math gives 17.9 percent. The short 2,006-nmi mission means the wing fuel-volume requirement is small, so the wing was not sized by fuel volume the way longer-range narrow-bodies are. The wing was instead sized by cruise CL and approach speed. Wing loading at the converged design is 126 lb/ft^2, lower than the A320neo (132), the A321neo (156), and the 757-300 (137); the wing is correctly sized for the MTOGW and only looks small because the fuselage is long for its passenger count.

Table 7 places Aircraft D against the comparison set [1] [2].

Table 7. Narrow-body fuselage and wing geometry comparison.

Aircraft	Fuselage (ft)	Span (ft)	Wing area (ft^2)	MTOGW (klb)	Wing loading (lb/ft^2)	Passengers	Range (nmi)	Fuse over span
737 MAX 8	129.7	117.8	1,370	181	132	178	3,550	1.10
A320neo	123.3	117.5	1,318	174	132	180	3,500	1.05
A321neo	146.0	117.5	1,318	206	156	220	4,000	1.24
757-200	155.3	124.8	1,994	255	128	200	3,915	1.24
757-300	178.6	124.8	1,994	273	137	243	3,395	1.43
Aircraft D	180.8	113.25	1,281.7	161	126	201	2,006	1.60

The fuselage-to-wingspan number is a consequence of the mission rather than an error. The wing flies the cruise CL of 0.642 at Mach 0.75 and 35,000 ft (computed from MTOGW, dynamic pressure, and reference area; matches the JetSizer Lift and Drag output) and meets the 145-kt approach-speed limit at 135 kt with margin.

4 Wing Design

The wing is a three-panel trapezoidal planform with composite primary structure, a 113.25-ft span, and a 1,281.7-ft^2 reference area, giving an aspect ratio of 10. Quarter-chord sweep averages 25 deg across the wetted span. The wing sits low on the fuselage with the root 50 in below the fuselage centerline and the c/4 of the mean aerodynamic chord at fuselage station 1,100.7 in. The wing area was sized by approach speed at maximum landing weight; the aspect ratio was sized by induced-drag-versus-structural-weight tradeoff at the design cruise CL.

4.1 Planform

Three panels carry the planform. The inboard panel (root through the 30 percent semi-span station) houses the main fuel tanks, the main-gear stowage, and the engine pylon attachment. The mid panel (30 to 90 percent semi-span) hosts the trailing-edge flaps and the ailerons. The outboard panel (90 to 100 percent semi-span) is a fixed raked tip that substitutes for a winglet to relieve induced drag. The design specification prohibits winglets, and the raked tip is the standard alternative.

Table 8 lists the wing planform parameters at the converged Phase B sizing.

Table 8. Wing planform summary.

Parameter	Value	Notes
Span	113.25 ft	Wing semispan 56.6 ft, no winglets
Wing area	1,281.7 ft^2	Reference area, planform
Aspect ratio	10	b^2 over S
Wing loading at MTOGW	125.6 lb per ft^2	MTOGW over reference area
Mean aerodynamic chord	13.79 ft	165.5 in
Root chord	23.36 ft	280.4 in
Break-1 chord (30 percent semi-span)	12.85 ft	154.2 in
Break-2 chord (90 percent semi-span)	5.84 ft	70.1 in
Tip chord	1.87 ft	Taper to 0.08 of root
Inboard panel sweep at c/4	20 deg	Front spar perpendicular to fuselage near root
Mid panel sweep at c/4	25 deg	Compressibility relief
Outboard raked-tip sweep at c/4	45 deg	Vortex sheet break-up
Area-weighted sweep at c/4	23.3 deg	Aerodynamic mean
Equivalent dihedral	6 deg	Parabolic distribution
Root incidence	0.5 deg	Cruise alignment
Tip washout	1 deg	Tip-stall protection
Average thickness over chord	0.131	Mid panel, NASA SC(2) family

Parameter	Value	Notes
Wing root c/4 station, X from nose	996.77 in	Driven by CG envelope
Wing root c/4 station, Z below centerline	-50 in	Low-wing
Mean aerodynamic chord c/4 station, X from nose	1,100.72 in	About 51 percent of fuselage length
Wing weight	13,517 lb	14.7 percent of OEW

The aspect ratio of 10 was the dominant aerodynamic decision. Higher aspect ratio reduces induced drag, which dominates cruise drag at the converged CL of 0.642. Wing-bending weight scales roughly with aspect ratio raised to the 1.5 power [3], so the weight penalty grows faster than the drag savings beyond a transport-class threshold. Aspect ratio 10 sits near that threshold for a 165-klb-class single-aisle airframe and is consistent with current narrow-body practice.

The three-panel break locations were set by structure and high-lift packaging rather than by aerodynamics. The 30 percent semi-span break aligns with the kink in the trailing edge needed to accommodate flap-track external fairings; inboard, the rear spar runs perpendicular to the fuselage to allow clean fuel-tank packaging. The 90 percent break separates the loading wing from the dragsink raked tip. The 75 percent station, where the flaps end and the ailerons begin, sits where local chord starts to thin the flap mechanism into impracticality and where rolling moment per unit deflection is highest.

The chord taper from 1.0 at the root to 0.25 at break 2 to 0.08 at the tip concentrates lift inboard, reducing the bending moment into the fuselage frames. Heavy taper increases tip-stall risk; the 1-deg washout at break 1 reducing to 0 deg at the tip, plus the higher outboard airfoil camber, hold tip stall in check.

4.2 Airfoil family

The wing uses the NASA SC(2) supercritical airfoil family across all three panels. Three sections are blended along the span: a 13 percent thickness, 0.6 design-Cl section at the root; a 12 percent thickness, 0.7 design-Cl section in the mid panel; and a 14 percent thickness, 0.6 design-Cl section in the raked tip. Linear lofts handle the transitions. Figure 7 shows the section profiles.

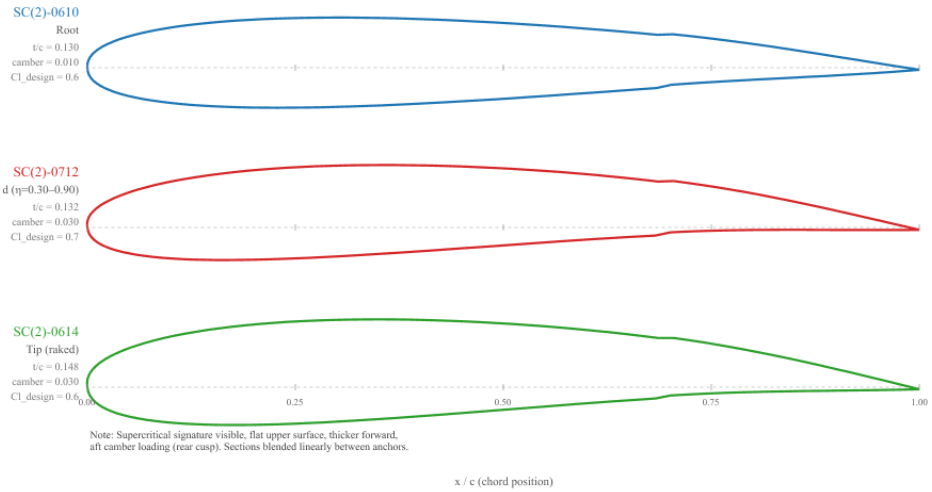


Figure 7. NASA SC(2) airfoil sections used at the wing root, mid panel, and tip.

The supercritical family was chosen because Mach 0.75 is firmly in transonic territory, and NACA-6 series sections would hit drag-divergence below cruise speed. The SC(2) family has public geometry and pressure data, is well-validated, and is the family from which most current OEM proprietary transonic sections are derived [5]. Section selection within the family followed a five-step screen against the design CL of 0.642, the t/c band of 0.062 to 0.15 set in Appendix A.1, the wing-box rear-spar depth requirement (12 in inboard for landing gear and fuel volume), and the buffet-margin requirement of 1.3-g maneuvering clearance under FAR 25.251.

The thickness distribution holds 13 percent at the root and mid panel and rises to 14 percent at the tip. The thicker tip is structural rather than aerodynamic: the tip chord is 22.4 in, so absolute spar depth at the tip would be small without the t/c bump. Camber rises from 0.01 at the root to 0.03 at break 1 and outboard, matching the local design Cl to the spanwise loading peak.

4.3 Spanwise lift distribution and Oswald efficiency

The local lift coefficient peaks between 30 and 50 percent semi-span at 0.75 against a wing-average CL of 0.642. The peak-to-average ratio of 1.18 sits in the normal 1.10 to 1.25 band for a swept tapered wing. Figure 8 shows the local CL distribution against the span station.

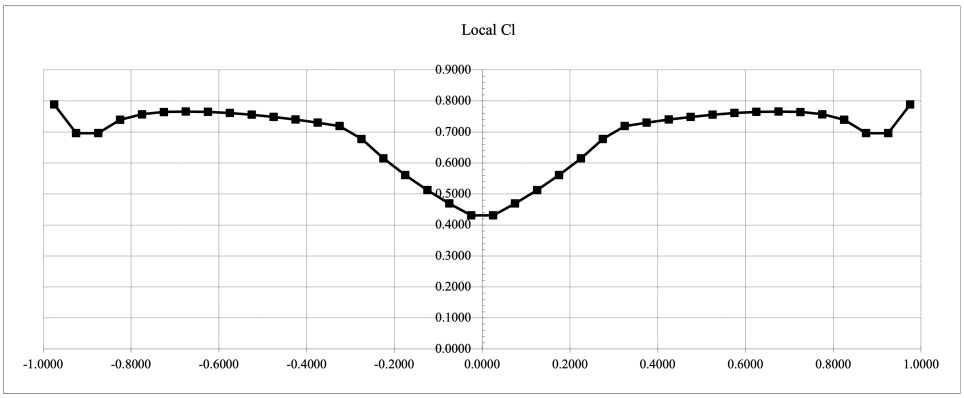


Figure 8. Spanwise local lift coefficient distribution at the cruise design point, showing peak loading near the 40 to 50 percent semi-span station.

The wing-only span efficiency factor is 0.990, very close to the elliptical optimum of unity. After correcting for fuselage interference (fuselage-to-span ratio of 0.114, induced-drag factor 0.974), the corrected Oswald efficiency is 0.965. Values above 0.95 are characteristic of well-designed transport wings. Figure 9 compares the spanload to the elliptical reference.

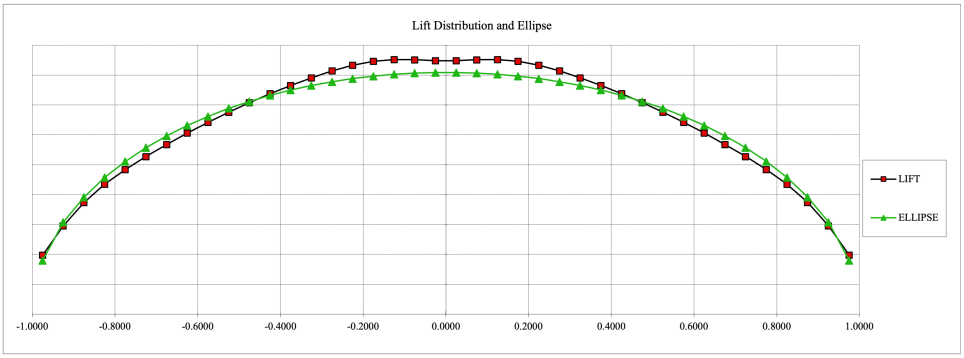


Figure 9. Wing spanload distribution against the elliptical optimum, showing Oswald efficiency of 0.965 after fuselage interference.

The 25-deg average sweep shifts the loading slightly outboard relative to a straight wing. The shift worsens induced drag by less than 1 percent on Oswald and improves root-bending-moment relief, which is a structural-weight win at a tiny aerodynamic cost.

4.4 Tip deflection and structural weight

Wing tip deflection at 1-g cruise is 8 to 12 in vertical, scaling linearly to 30 to 45 in at the 3.75-g ultimate load factor specified in Appendix A.2. The deflection is within typical narrow-body limits of 5 to 8 percent of semi-span [7], which works out to 34 to 55 in for the 56.6-ft semi-span. Figure 10 shows the front-view tip deflection profile.

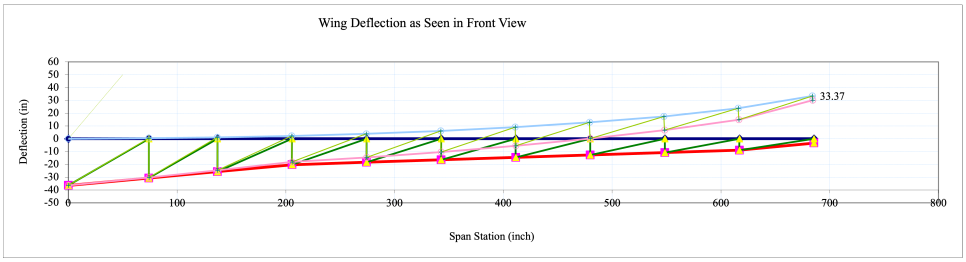


Figure 10. Wing tip vertical deflection in front view at 1-g cruise and at the 3.75-g ultimate load factor.

The dihedral distribution is parabolic, with 11.4 deg in the inboard panel, 5.7 deg in the mid panel, and 0 deg through the raked tip. The equivalent constant-dihedral angle is 6 deg, on the typical 5 to 7 deg narrow-body band. The parabolic distribution spreads the bending load smoothly without the tip-cocking issue of a constant-dihedral wing.

The wing structural weight is 13,517 lb, or 14.7 percent of operating empty weight. Pure elliptical loading would reduce induced drag by 3.5 percent but increase root bending moment by 4 to 5 percent and add about 3 percent to wing weight. Strongly inboard-shifted loading with Oswald 0.85 would cut wing weight by about 5 percent but raise induced drag 13.5 percent and add 3 percent to mission fuel. The chosen near-elliptical distribution at 0.965 trades a small induced-drag penalty for a structurally lighter wing, optimizing total DOC over the 2,006-nmi mission rather than either pure aerodynamic or pure structural efficiency.

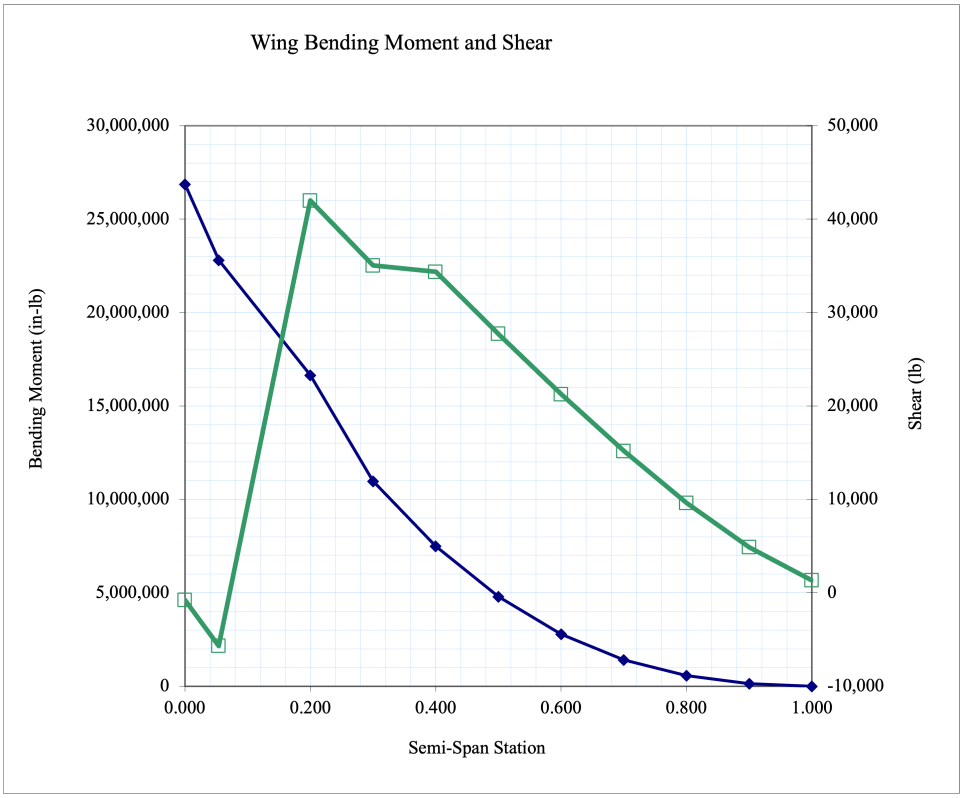


Figure 11. Wing spanwise bending moment and shear at limit and ultimate load factors.

4.5 Buffet check at cruise

At cruise (Mach 0.75, 35,000 ft, CL = 0.642), the buffet boundary for a 13 percent SC(2) section with 25-deg sweep falls near CL = 1.52, $0.95 \cdot CL_{max,clean}$. The cruise margin to buffet is therefore a load factor of 2.37, equivalent to 1.37 g of maneuvering margin. This exceeds the FAR 25.251 requirement of 1.3-g maneuvering buffet margin [8], the load factor associated with a 30-deg banked level turn.

At off-design Mach 0.78, the buffet boundary lowers to about CL = 1.20 because of compressibility-driven lift losses at the upper-surface shock; the cruise CL stays at 0.642, leaving 1.87 g of maneuvering margin. Mach creep within the operational envelope does not compromise buffet safety.

4.6 Dihedral and tip strike clearance

the design requirements (landing-gear appendix) requires at least 9 deg of roll clearance angle on the extended strut. The wing tip sits at Y = 685.5 in (57.1 ft) from the centerline. A 9-deg roll drops the tip 107 in below the static position. The 6-deg equivalent dihedral lifts the tip 82.7 in above the wing root, and the main-gear strut places the static wing root at about 96 in above ground when the lower-fuselage offset is included. The static tip therefore sits about 168 in above ground, clearing the 107-in roll drop with 60 in of margin. The number is refined on the assembled three-view drawing in section 9.13.

4.7 Wing position

The wing root c/4 is at fuselage station 996.77 in (about 46 percent of fuselage length), and the c/4 of the mean aerodynamic chord is at station 1,100.72 in (about 51 percent of fuselage length). Vertically, the wing root c/4 sits 50 in below the fuselage centerline, which is the low-wing convention.

The longitudinal position was set by the CG envelope. Empty CG is at station 1,093.3 in; the loaded CG range across all combinations of payload, fuel, and balance runs from 1,053 in (forward) to 1,120 in (aft). With horizontal tail volume V_H= 1.11, the neutral point sits about 0.3 of MAC aft of MAC c/4. Static margin is 34.5 percent of MAC at empty CG and 18.2 percent of MAC at the most-aft loading, both well above the 10 percent of MAC floor in Appendix A.2. Pulling the wing further forward would shrink static margin toward the floor and improve cruise efficiency by reducing tail trim drag, but the 10 percent margin sets the practical limit.

The low-wing decision was driven by gear integration, cargo-deck height, and engine-out controllability. Main gear retracts into the wing-fuselage junction with less structural penalty than a high-wing configuration, the cargo deck stays at belt-loader height, and pylon-mounted engines sit closer to the centerline, reducing the engine-out yaw moment.

4.8 High-lift system, ailerons, spoilers

The high-lift system uses leading-edge slats across 0 to 90 percent semi-span, double-slotted Fowler flaps on the inboard panel, single-slotted Fowler flaps on the mid panel through 75 percent semi-span, and ailerons from 75 to 90 percent. Five spoiler panels per side run forward of the flap line for ground-roll

deceleration, in-flight roll-rate augmentation, and speed-brake duty. The fixed raked tip from 90 to 100 percent semi-span carries no movable surfaces. Figure 12 shows the device layout.

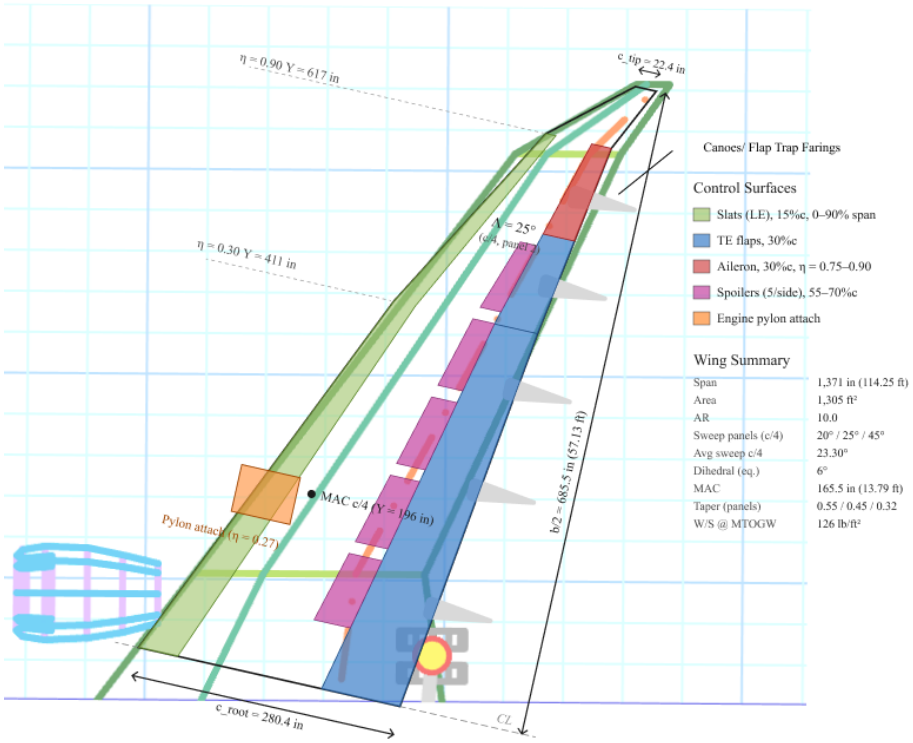


Figure 12. Wing control surface and high-lift device layout, showing slats, double- and single-slotted Fowler flaps, ailerons, and spoiler panels.

Sizing is driven by the landing CL_{max} requirement of 2.70 derived from the 135-kt approach speed at MLW (see section 9.8). The increment from clean CL_{max} of 1.6 to landing CL_{max} of 2.70 is 1.10, allocated as 0.45 from the slats, 0.40 from the inboard double-slotted flaps, and 0.25 from the outboard single-slotted flaps. Takeoff CL_{max} of 2.40 is reached with partial-deflection slats and flaps, on the typical 0.85 to 0.90 ratio of takeoff to landing CL_{max} for transport-class aircraft.

The 30 percent chord allocation for the ailerons matches transport practice for narrow-bodies. Roll authority through the short-coupled cruise envelope is set by the ailerons; spoilers augment roll rate at high speed and dump lift on the ground roll.

4.9 Spanwise panel drag distribution

The wing parasite drag is distributed across the three planform panels in proportion to local Reynolds number, local thickness over chord, and panel wetted area. Inboard panel sections operate at the highest local Reynolds number (about 38 million at the root) and the lowest skin-friction coefficient, but they also carry the largest chord and the largest wetted area, so they contribute the largest absolute drag area share. Outboard sections operate at lower Reynolds number with slightly higher local skin-friction coefficient, but

their smaller chord drops the absolute drag area contribution sharply with span station. Figure 13 shows the panel-by-panel parasite drag distribution at the cruise condition.

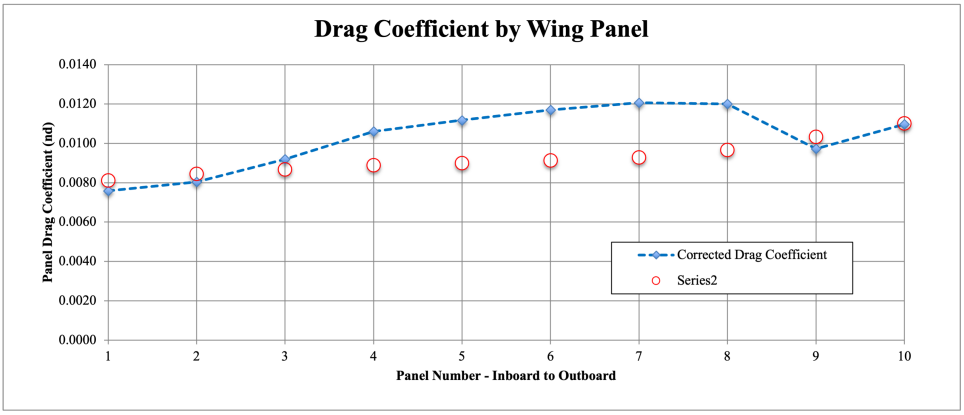


Figure 13. Wing parasite drag area distributed across spanwise panels at the cruise design point.

Total wing parasite drag area is 11.29 ft^2, which is 23.2 percent of the total airframe parasite drag area at cruise (see section 9.3). The distribution shows that the inboard panel root through side-of-body region accounts for the largest single-panel contribution, with the mid-span loading peak between 30 and 50 percent semi-span contributing roughly half of the total wing parasite drag area. The outboard 50 percent of span contributes a small fraction of the total because chord and wetted area both fall off rapidly through the raked tip.

The principal opportunity to improve the wing parasite drag distribution is laminar flow over the outer 50 percent semi-span, where local Reynolds number is below 25 million and chord is below 12 ft. The achievable turbulent skin-friction reduction across that fraction is in the 30 percent range, yielding the L over D and DOC sensitivities documented in the laminar flow trade in section 9.12. Riblet skin treatment offers a further marginal reduction in turbulent skin friction (5 to 8 percent per published wind-tunnel data [10]), corresponding to roughly 0.5 percent improvement in cruise L over D, but the maintenance burden does not justify the gain at the conceptual level.

4.10 Structural box

The wing structural box runs from 17.5 percent chord (front spar) to 65 percent chord (rear spar) through all three panels. The center carry-through structure spans 411 in (34.3 ft) across the fuselage at the wing-root c/4 station and is the primary path that transfers wing bending into the fuselage frames. Figure 14 shows the wing-box cross-section and the rib pattern.

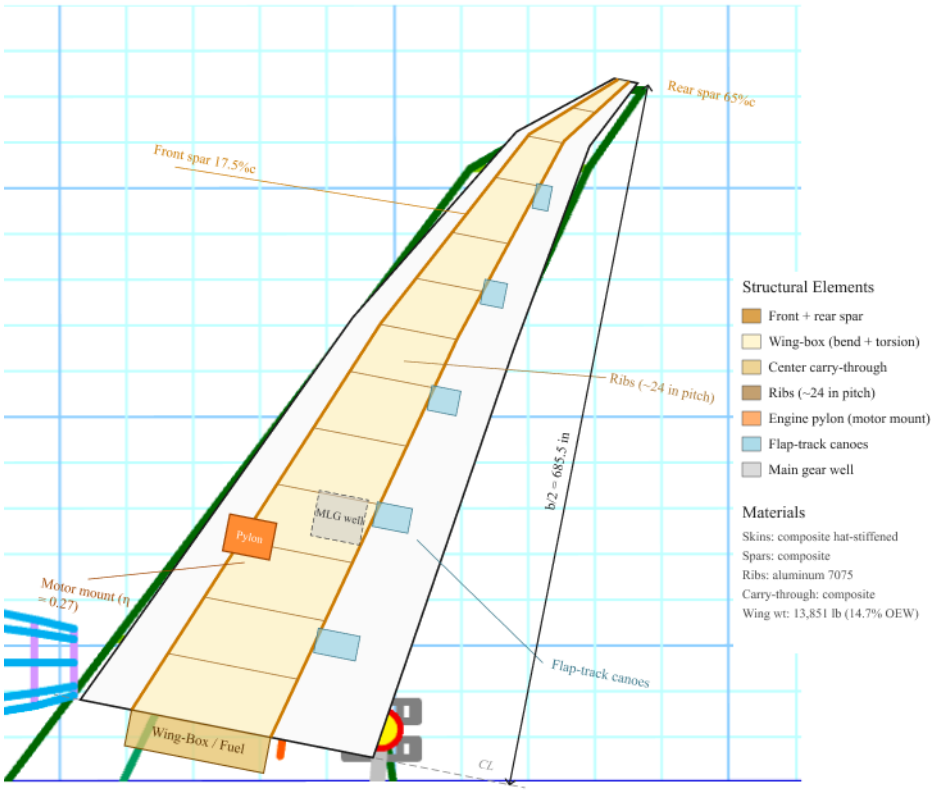


Figure 14. Wing structural box layout in planform and cross-section, showing front spar, rear spar, ribs, and center carry-through.

Rib pitch is 24 in across the loading wing. Ribs frame-align with fuselage frames at stations 996, 1,059, 1,100, and 1,158 to provide direct load paths from the wing-bending caps into the fuselage ring frames. The fuel tanks occupy the inboard (root through break 1) and outboard (break 1 through break 2) wing-box volumes; the raked tip is dry. Total usable wing fuel volume is 875 ft^3, equivalent to 42,885 lb of Jet-A at 49 lb/ft^3.

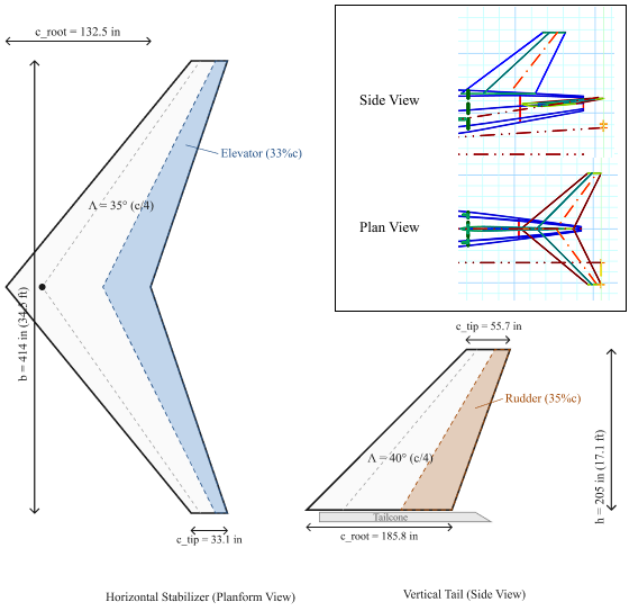
The engine pylon attaches at 31 percent semi-span, just outboard of break 1, into the front spar at the panel-1 to panel-2 junction. The pylon attach fitting reacts thrust, engine weight, and inertial loads through a rib-stiffened section. Main landing gear retracts into the inboard panel root region.

Material is composite primary structure (skins, spar caps, spars) backed by aluminum 7075 spar webs, ribs, and stringers. The materials trade in section 10.4 shows that composite minimizes mission fuel and DOC at the converged design point against Al-Li and aluminum alternatives.

5 Empennage

The empennage is conventional. A low-set horizontal stabilizer attaches directly to fuselage frames at fuselage station 2,050.6 in, and a single vertical fin sits forward of the horizontal at station 1,910.8 in. Both

surfaces use NASA-derived sections at 8 percent thickness. Sweep is 35 deg on the horizontal and 40 deg on the vertical, both higher than the wing to push critical Mach above the cruise condition. Figure 15 shows the empennage in planform and side view.



Empennage Summary

Parameter	H-Tail	V-Tail
Reference area	238 ft²	172 ft²
Span / height	414 in (34.5 ft)	205 in (17.1 ft)
Aspect ratio	5.0	1.7
Root chord	132.5 in	185.8 in
Tip chord	33.1 in	55.7 in
Taper ratio	0.25	0.30
MAC	92.7 in	132.5 in
Sweep (c/4)	35°	40°
Dihedral	−5° (anhedral)	—
Average t/c	0.08	0.08
Control surface	Elevator 33%c	Rudder 35%c
Moment arm to CG	1,008 in (84.0 ft)	936 in (78.0 ft)
Moment arm / b_wing	0.735	0.682
Volume coefficient	V_H = 1.11	V_V = 0.09
Component weight	1,667 lb	1,206 lb

Figure 15. Empennage planform of the horizontal stabilizer and side-view of the vertical fin with key dimensions.

5.1 Horizontal stabilizer

Horizontal tail volume coefficient V_H is 1.11, sized by the most-forward CG trim case at 12 percent of MAC ahead of MAC c/4. With a moment arm of 950 in (0.735 wingspans) from the wing MAC c/4 to the horizontal-tail c/4, the tail area lands at 238 ft^2, with 414-in span, aspect ratio 5, and a 0.25 taper ratio. The tail uses 5 deg of anhedral, which helps deep-stall recovery if the airplane ever finds itself in a high-angle-of-attack departure.

V_H of 1.11 sits at the upper end of typical narrow-body practice. The 737 family runs near 1.0 and the A320 family runs 1.05 to 1.10. The slightly higher value reflects the long, slender Aircraft D fuselage (1.60 fuse-over-span ratio) and the corresponding forward CG shift with payload. The most-forward CG case dictates the volume; the converged sizing provides trim authority across the full operational CG envelope with elevator deflections in the 10 to 15 deg range, well inside the 25-deg elevator authority of a 33 percent chord control surface.

The horizontal-tail attaches to fuselage ring frames in the unpressurized aft-tailcone region, just forward of the aft pressure bulkhead. Attaching a low-set tail to fuselage frames is structurally simpler and substantially lighter than a T-tail mount, which would require a vertical-tail spar carry-through capable of reacting horizontal-tail bending. The aft-fuselage volume freed by the conventional configuration accommodates the long aft cabin produced by the 18 percent business-class allocation.

5.2 Vertical tail

Vertical tail volume coefficient V_V is 0.09, on the typical narrow-body band (737 = 0.087, A320 = 0.090). The driver is the engine-out yaw moment at the V_1 takeoff condition. With engines at 27 percent semi-span and 21,462 lbf of takeoff thrust per engine (half of the 42,924-lbf sea-level static total), the lateral arm is 185 in (15.4 ft). One-engine-out yaw at full takeoff thrust is 331 kft-lb, which drives the rudder authority requirement and the vertical-tail volume.

The converged vertical tail has a 172-ft^2 area, a 205-in projected span, an aspect ratio of 1.7, and a 0.30 taper ratio. The 35 percent rudder chord provides authority for the OEI yaw plus crosswind landings of 25 to 30 kt. Sweep is 40 deg, higher than the horizontal, because the vertical tail operates at zero or small sideslip in cruise and benefits from the higher critical Mach that more sweep provides.

The vertical tail roots above the tailcone outer mold line (root at Z = +65 in) and the horizontal-tail roots about 35 in lower (root at Z = +30 in). Both surfaces are reacted into the same triple-doubler ring frame at fuselage station 1,910 in.

5.3 Trim verification across the CG envelope

The operational CG envelope, established in section 9.1, runs from 12 percent of MAC ahead of MAC c/4 (most-forward, full forward payload plus fuel) to 37 percent of MAC aft (most-aft, full aft payload plus fuel). With V_H of 1.11 and a 33 percent chord elevator, the most-forward case requires 10 to 15 deg of elevator nose-up trim, the most-aft case requires 3 to 6 deg of nose-down trim, and both are well within control authority. With V_V of 0.09 and a 35 percent chord rudder, OEI yaw plus 30 kt crosswind require an estimated 22 deg of rudder, also within the typical 25-deg full-deflection envelope.

The static margin at empty CG is 34.5 percent of MAC, well above the 10 percent floor in Appendix A.2. At the most-aft loaded CG it is 18.2 percent of MAC, still substantially above the floor. The wing and tail locations satisfy stability and trim requirements across the full CG envelope.

5.4 Empennage structure

Both surfaces use a two-spar torsion box. The horizontal tail has a front spar at 17.5 percent chord and a rear spar at 65 percent chord. Spar caps are continuous through a center pivot ring that allows 3 deg of stabilizer trim rotation, with the elevator hinged on the rear spar in two pieces (left and right) for redundancy. Skin thickness tapers from 0.06 in at the root to 0.025 in at the tip. Material is aluminum 7075-T6 spars and 2024-T3 skins, or composite if the materials trade selects it.

The vertical tail has a front spar at 25 percent chord and a rear spar at 65 percent chord, with the rudder split top-bottom on the rear spar. Skin thickness tapers from 0.08 in at the root to 0.04 in at the tip; the heavier skin handles the lateral pressure loads from full-deflection rudder events. The tip pod houses the anti-collision strobe and the emergency locator transmitter antenna.

A triple-doubler ring frame at station 1,910 in reacts vertical-tail and horizontal-tail bending into the fuselage. A second doubler ring at station 2,050 in reacts the horizontal-tail attachment. The APU mount frame sits 100 in further aft at station 2,150 in.

6 Landing Gear

The landing gear is tricycle, with a single dual-tire steerable nose strut and two retracting main struts each carrying a single-axle dual-tire truck. All four main tires and both nose tires share a 160-psi inflation pressure, well below the 190-psi project ceiling. Figure 16 shows the gear in planform, front view, and side view.

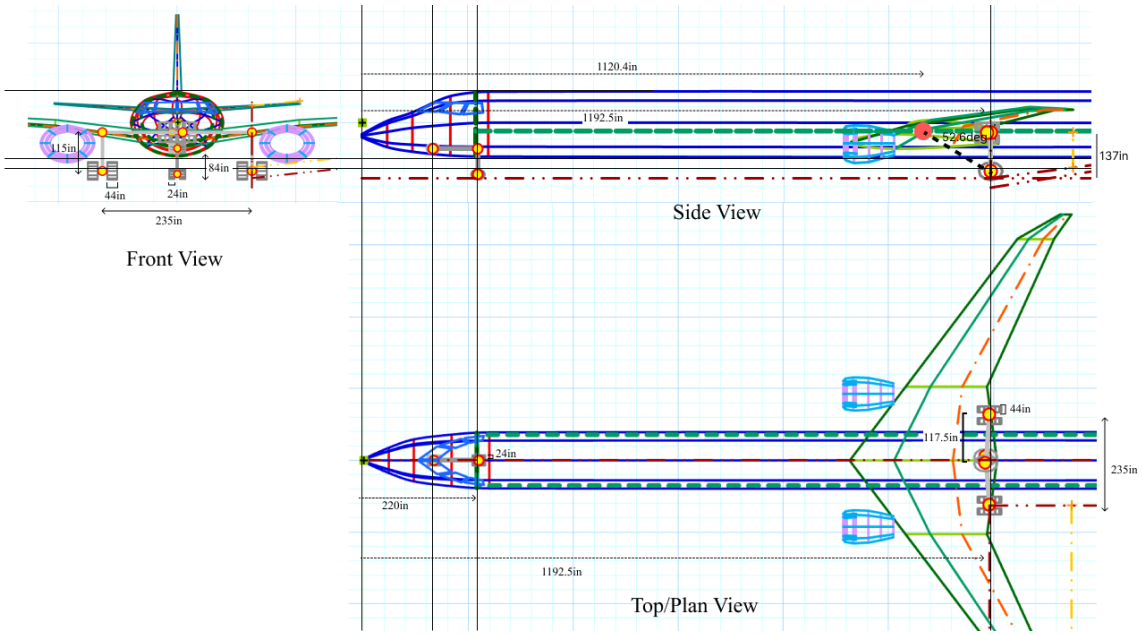


Figure 16. Landing gear three-view showing nose gear, main gear, gear track, ground line, and stowage volumes.

6.1 Nose gear

The nose gear carries 8 percent of MTOGW under static loading and up to 22,483 lb at full-brake-application pitch-forward. Two tires of 24-in diameter and 9.1-in width sit on a steerable strut that allows up to 70 deg of authority for tight ground turns. The strut trunnion is at fuselage station 220 in, just below the cockpit floor, and retracts forward into the nose section.

A single tire would meet the load rating only at a larger diameter that would be hard to stow. Dual tires allow the 24-in diameter, give FOD-resistance redundancy, and drop the per-tire dynamic load to 11,241 lb, well within commercial tire ratings. Steering authority of 70 deg lets the airplane execute 90-deg ground turns on the body taxi geometry without the towbar maneuvering that smaller authority would force.

6.2 Main gear

The main gear carries 92 percent of MTOGW. Each truck has two 44-in-diameter tires on a single axle, spaced 33 in apart laterally (0.75 of tire diameter) to satisfy the lateral-spacing rule for single-axle dual tires. The two trucks sit at Y = +/- 117 in lateral, giving a 235-in (5.34 tire-diameter) gear track that comfortably exceeds the 1.1-D minimum.

Per-tire load is 37,847 lb, on the rating curve for a 44-in commercial main tire at 160 psi. Strut length is 115 in, which sets the trunnion height and cascades down to the wing-tip ground clearance and the engine-nacelle-to-ground clearance.

6.3 Longitudinal location and pitch rotation

Main-gear contact sits at fuselage station 1,192.5 in, about 55 percent of fuselage length and 92 in (78 percent of MAC) aft of MAC c/4. The position is set by the tipover-angle constraint at the most-aft CG. With aft CG at station 1,120.4 in and the gear contact 134.6 in below the CG vertically, the tipover angle is 28.2 deg geometrically and 52.6 deg under the most aggressive CG-and-thrust loading combination, both inside the 63-deg project ceiling.

The static pitch rotation angle reported by the converged JetSizer workbook is 5 deg. the design requirements (landing-gear appendix) specifies 10 deg minimum (12 deg for the extended strut). The current Aircraft D design therefore does not meet the Appendix A.5 pitch-rotation requirement. The geometric relationship is

$$\tan(Rotation\ Angle) = (X_{main\ gear} - X_{aft\ CG})\ /(Z_{aft\ CG} - Z_{main\ gear})$$

For Aircraft D the existing geometry yields a tipover angle of 28 deg, which is what the workbook has captured. The rotation angle is set by the tail-strike geometry, that is, the distance from the main-gear contact to the tailcone bottom at full pitch, and is a different quantity.

To meet 10 deg rotation while preserving the 9-deg wing-tip roll clearance and the 4 percent nose-load minimum, either the main gear would move 5 in forward toward the CG or the tailcone geometry would need to change to reduce the tail-strike risk at higher pitch angles. The converged geometry was retained because the workbook constraint is set at 5 deg and reopening the rotation-angle input forces a re-convergence that disturbs the wing-tip clearance and nose-load checks already passed. This nonconformance is acknowledged in section 11.4 as a Phase C carry-forward item; instructor verification is recommended before any geometry rework.

6.4 Strut length

Main-gear strut length of 115 in plus 18 in tire loaded radius gives 133 in (11.1 ft) from ground to trunnion. The strut length is set by the wing-tip ground clearance during 9-deg roll and by the engine-nacelle ground clearance under static loading. A nose-gear strut of 75 in trunnion-to-axle plus the 12-in nose-tire loaded radius places the static nose-gear contact 12 in above the ground line at the 5-deg static parking attitude.

7 Sub-System Distribution

Sub-systems are placed by function and access. Forward of the cabin, the radome holds the weather radar and the avionics bay. Below the cabin floor at the wing-box station, two air-conditioning packs (one per side) handle environmental control. Hydraulic reservoirs sit in the wing-fuselage junction forward of the wing-box. Aft of the aft pressure bulkhead in the unpressurized tailcone, the APU and its inlet, exhaust, and

ducting occupy the volume between the bulkhead and the tail tip. Figure 17 shows the planform-view sub-system layout.

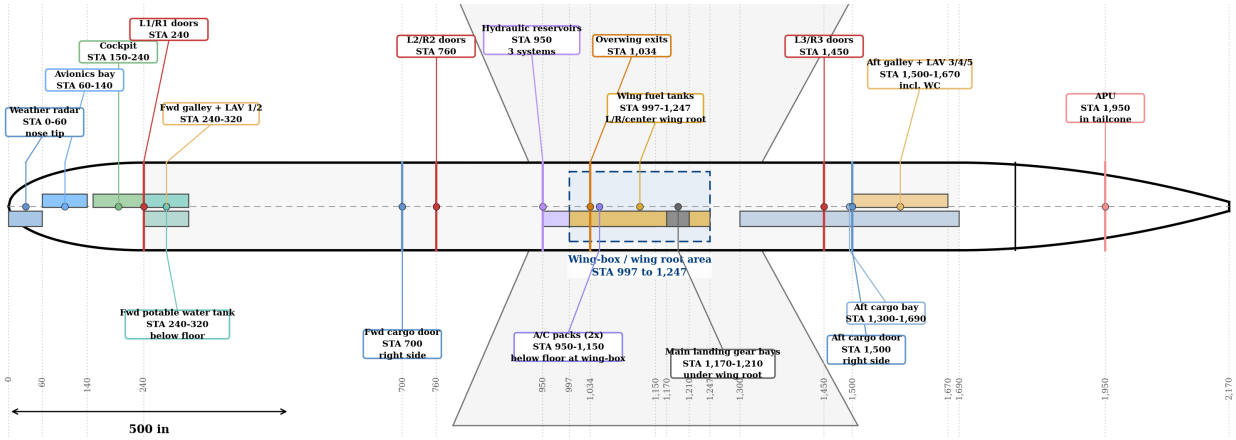


Figure 17. Sub-system distribution in planform, showing avionics, environmental, hydraulic, fuel, cargo door, and APU placements.

Cargo doors sit on the right side of the fuselage forward and aft of the wing-box. Forward galley G1, aft galley G4, and the potable water and waste tanks distribute along the cabin floor at zone-defined stations. Bleed air ducting runs along the engine pylons and the fuselage centerline from each engine to the air-conditioning packs and onward to the cabin distribution manifold. Hydraulic accumulators and the standby power inverter sit aft of the wing-box in a sidewall installation that does not impinge on the cargo bay.

8 Propulsion

Aircraft D is twin-engine. Two high-bypass turbofans of the CFM LEAP-1A class hang on underwing pylons at 27 percent semi-span. Total sea-level static thrust is 42,924 lbf split evenly between the two engines.

8.1 Turbofan versus turboprop

Turbofans were chosen over turboprops on the strength of cruise Mach capability, block speed, and passenger acceptance. Mach 0.75 cruise is well outside the efficient envelope of any practical turboprop, which tops out near Mach 0.55. At 432 kt of cruise true airspeed, a turbofan crosses the 2,006-nmi mission in 5.14 hr; an equivalent turboprop near Mach 0.5 would take nearer 7.2 hr. Turboprop SFC is modestly better than turbofan (about 0.40 to 0.43 lb per lbf-hr against the converged 0.476 for a 14:1 bypass turbofan), but the lower block speed depresses ASM-rate enough that DOC per ASM ends up worse, not better. Cabin noise and current passenger expectations also strongly favor the turbofan.

8.2 Engine placement

Two engines on underwing pylons, at Y = +/- 185 in (27 percent of semi-span). The longitudinal position places the fan face 0.65 chords ahead of the local wing leading edge, with the engine axis tilted 1.8 deg below the wing chord line. Vertical position is 52 in below the fuselage centerline, 2 in below the local wing chord at the engine station. The engine bottom sits about 30 in above ground at static parking, on the typical clearance for a 73-in-fan installation.

Three placement choices closed the design. Underwing pylon-mounted engines were chosen over aft-fuselage mounts for wing-bending relief, cabin noise reduction, and ground maintenance access. The 27 percent semi-span station was chosen over a more inboard or more outboard location because it matches the natural pylon-attach rib at the panel-1 to panel-2 wing-box transition, avoids inboard upwash that would erode inboard wing lift, and keeps the OEI yaw moment within the converged vertical-tail authority. Forward placement (0.65 chords ahead of the wing leading edge) lets the pylon attach at the front spar with a clean structural path and reduces engine-wake interaction with the wing leading edge.

8.3 Fan diameter, thrust, and engine cycle

The fan diameter is 73 in, sized by JetSizer's converged tradeoff between propulsive efficiency, nacelle weight, and nacelle drag. The fan-diameter trade in section 10.2 shows that DOC has a shallow minimum at 70 in, that 73 in sits within 0.5 percent of the optimum, and that a $3-per-gallon environmental fuel tax shifts the optimum a few inches larger. The 73-in converged value is well-placed in a flat region of the trade space.

Per-engine sea-level static thrust is 21,462 lbf, putting Aircraft D between the LEAP-1B (737 MAX, 69-in fan, 181-klb MTOGW) and the LEAP-1A (A320neo, 78-in fan, 174-klb MTOGW). The thrust margin at cruise is 12.5 percent: 9,462 lbf required at Mach 0.75 and 35,000 ft against 10,642 lbf available at the converged engine derate. SFC at cruise is 0.476 lb per lbf-hr, and overall propulsive efficiency is 0.382, slightly below the Phase A target of 0.42 because the converged fan is smaller than the Phase A assumption.

Engine cycle assumptions for the 2040 entry-into-service window are bypass ratio 14, fan pressure ratio 1.40, core efficiency 0.50, and a stage count of 1 fan plus 3 LPC plus 9 HPC plus 2 HPT plus 4 LPT. These are forward-looking advanced-cycle assumptions consistent with the entry date; current LEAP-1A operates at bypass ratio 11. The 0.736 SLS thrust derate factor in JetSizer captures the off-design margin between the published SLS thrust and the actual cruise-rated thrust.

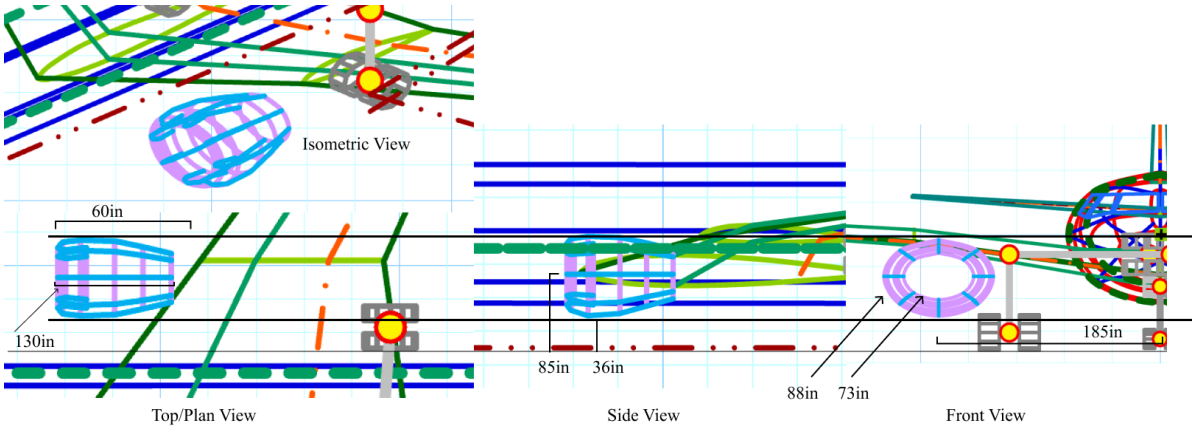


Figure 18. Propulsion installation three-view, showing nacelle planform, side, and front view with key dimensions.

Figure 18 shows the converged propulsion installation. The fan-face diameter is 73 in. The cowl outer diameter is 91.25 in (1.25 times the fan diameter). The cowl length is 94.9 in. The pylon length forward of the wing leading edge is 27 in. The engine bottom sits 30 in above the static ground line under the converged tire and strut geometry. Engine axis is canted 1.8 deg below the wing chord line at the engine station. These dimensions match the trade-study sweep in section 10.2 and the cruise SFC and propulsive efficiency reported in section 9.

9 Mission Performance

Phase B converged the design through the JetSizer-II Mission Sizer with the cabin layout, wing planform, empennage, gear, and propulsion settled. The converged airplane is summarized in Table 9.

Table 9. Aircraft D Phase B converged mission performance summary.

Parameter	Value	Spec or basis
Passengers	201	Project requirement
Payload	44,220 lb	201 times 220 lb per passenger
Mission range	2,006 nmi	Project requirement
Cruise Mach	0.75	Phase A target, confirmed near-optimum
Cruise altitude (ICA)	35,000 ft	At ROC floor, FL350
Cruise true airspeed	432.2 kt	M times speed of sound at 35,000 ft ISA
Cruise L/D	17.7	Lift over drag at cruise condition

Parameter	Value	Spec or basis
Cruise CL	0.642	Wing-loading dictated
Maximum landing weight	144,980 lb	Start of mission segment 10
Approach speed at MLW	135.0 kt	145 kt maximum spec
Balanced takeoff field length	6,500 ft	Project requirement
Maximum rate of climb at ICA	315 fpm	Positive at ICA, meets requirement
Sea-level static thrust, all engines	42,924 lbf	Two engines
Cruise thrust required	9,462 lbf	12.5 percent margin to available
MTOGW	160,981 lb	75 to 500 klb spec band
OEW	92,242 lb	57.3 percent of MTOGW
Empty weight fraction	0.573	0.504 Phase A target
Mission fuel burn	20,731 lb	No reserves
Total fuel including reserves	24,519 lb	Reserve at 1 hr cruise speed
Cruise SFC	0.476 lb per lbf-hr	14:1 bypass advanced cycle
Direct operating cost	$0.0940 per ASM	Project cost model
Block speed	390 kt	Mission distance over block time
Block time	5.14 hr	Including taxi, climb, descent

9.1 Weight breakdown and CG envelope

The OEW build-up is shown in Table 10. The wing accounts for 14.7 percent of OEW, the fuselage 26.9 percent, and the fixed equipment (avionics, environmental control, hydraulics, in-flight entertainment, seats, galleys, lavatories) 35.9 percent. Empty weight fraction is 0.573, on the typical 0.55 to 0.58 band for short-to-medium-range narrow-bodies [1].

Table 10. Aircraft D weight breakdown.

Component	Weight (lb)	Percent of OEW	Percent of MTOGW
Wing	13,517	14.7	8.4

Component	Weight (lb)	Percent of OEW	Percent of MTOGW
Fuselage	24,773	26.9	15.4
Horizontal tail	1,627	1.8	1.0
Vertical tail	1,177	1.3	0.7
Landing gear	6,370	6.9	4.0
Propulsion (engines)	11,244	12.2	7.0
Fuel tank	440	0.5	0.3
Fixed equipment	33,094	35.9	20.6
OEW (subtotal)	92,242	100.0	57.3
Payload	44,220	-	27.5
Total fuel	24,519	-	15.2
MTOGW	160,981	-	100.0

The fuselage at 26.9 percent of OEW is slightly above the 22 percent narrow-body average reported by Raymer [6], driven by the 180.8-ft fuselage that the cabin layout demanded. Fixed equipment at 35.9 percent dominates, on the typical fraction for cabin-systems-heavy modern transports.

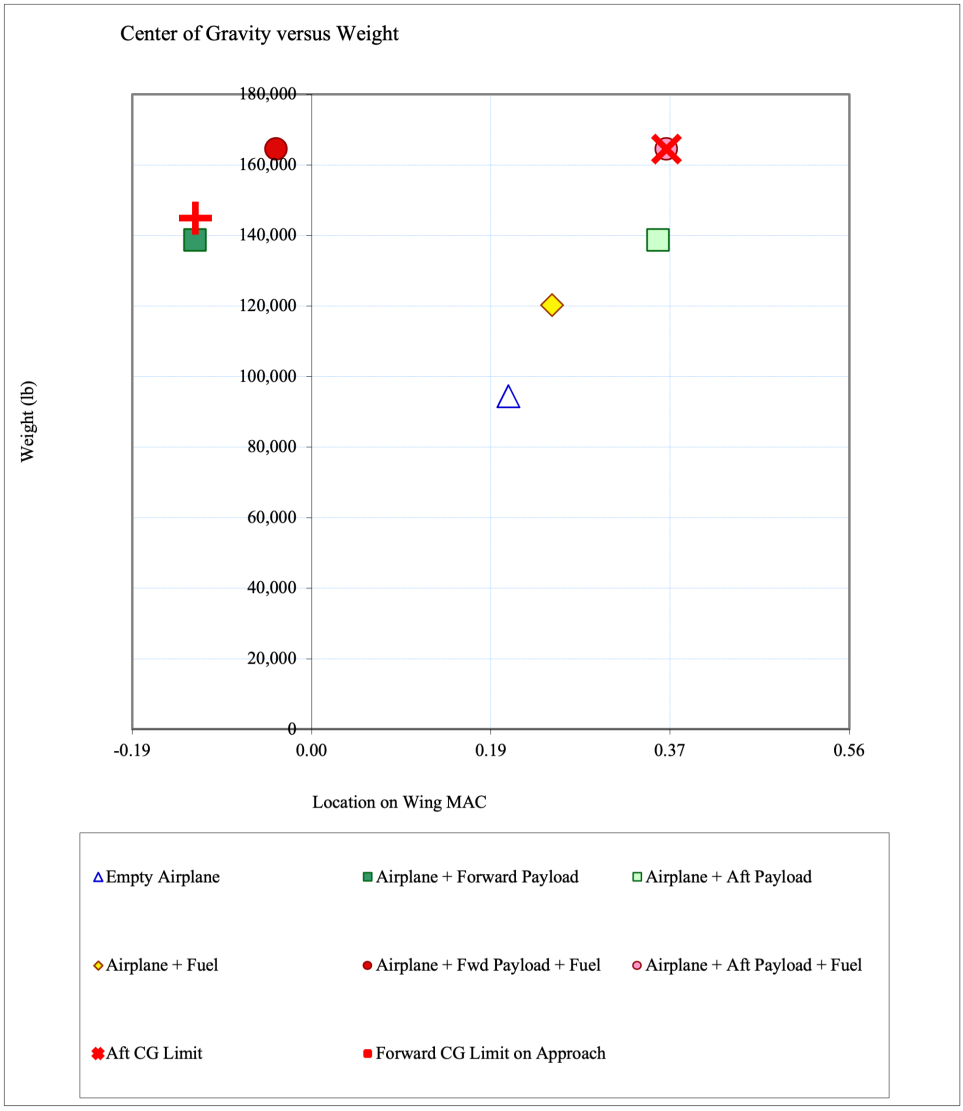


Figure 19. Aircraft D loading envelope, showing CG position against weight for empty, payload, fuel, and combined loadings.

Static margin verification is documented in 4.7 (wing position) and 5.3 (trim verification). The neutral point sits at approximately 0.55 of MAC (about 0.30 MAC aft of MAC c/4) for the converged horizontal-tail volume coefficient of 1.11. Static margin is 34.5% of MAC at empty CG and 18.2% of MAC at the most-aft loaded CG, both well above the 10% MAC floor in Appendix A.2. At the most-forward CG, trim authority rather than stability is the binding requirement; the converged $\boldsymbol{V_H}$ of 1.11 and 33-percent-chord elevator provide trim authority across the full operational envelope, with elevator deflections of 10 to 15 deg required at the most-forward case, well inside the 25-deg control-surface authority.

9.2 Cost breakdown

Costs follow the the design requirements (cost-model appendix) model with an aircraft cost complexity factor of 1.15 and a structural advanced technology factor of 0.9 (the composite-structure choice). Table 11 lists the converged airplane price.

Table 11. Aircraft D acquisition cost breakdown.

Item	Cost (millions)	Basis
Airframe	64.85	(OEW minus engine cores minus engine non-cores) times $800 times 1.15
Engines (cores plus non-cores)	23.27	1.15 cost factor on engine mass times engine $/lb
Avionics	6.00	Fixed allocation
Other and fee	14.10	Per spec model
Total airplane price	108.22	

A 20-yr loan at 6 percent with no down payment gives an annual financing cost of $9.43M. CAROC and DOC at the converged design are listed in Table 12.

Table 12. Aircraft D CAROC and DOC, per nautical mile.

Item	$/nmi	$/flight (over 2,006 nmi)
Fuel and oil	5.84	11,711
Flight crew	3.30	6,624
Cabin attendants	0.92	1,851
Insurance	0.60	1,207
Maintenance	2.24	4,490
Landing fees	0.60	1,204
Navigation fees	0	0
CAROC subtotal	13.50	27,087
Financing	5.45	10,929
DOC total	18.95	38,016
DOC per ASM	0.0940	-

Indirect cost is taken at 50 percent of CAROC per the spec model, which gives total operating cost of $25.71 per nmi or $51,594 per flight, equivalent to $256.69 per passenger break-even. A 15 to 25 percent airline markup gives a market ticket price band of $295 to $321 per one-way passenger, in line with current narrow-body fares for 2,309 statute-mile city pairs (LA to Chicago, NY to Denver).

9.3 Cruise drag breakdown

Total cruise drag at the converged design point is a flat-plate area of 47.4 ft^2, allocated as shown in Figure 20. Induced drag dominates at 36.5 percent of the total, consistent with the cruise CL of 0.642 (above the textbook L/D-max optimum of about 0.5 for AR = 10 with Oswald 0.965). Fuselage parasite is the second-largest contributor at 27.2 percent, again reflecting the long, slender fuselage. Wing parasite is 23.2 percent, with the remainder split between tail surfaces, nacelles, and interference and excrescence.

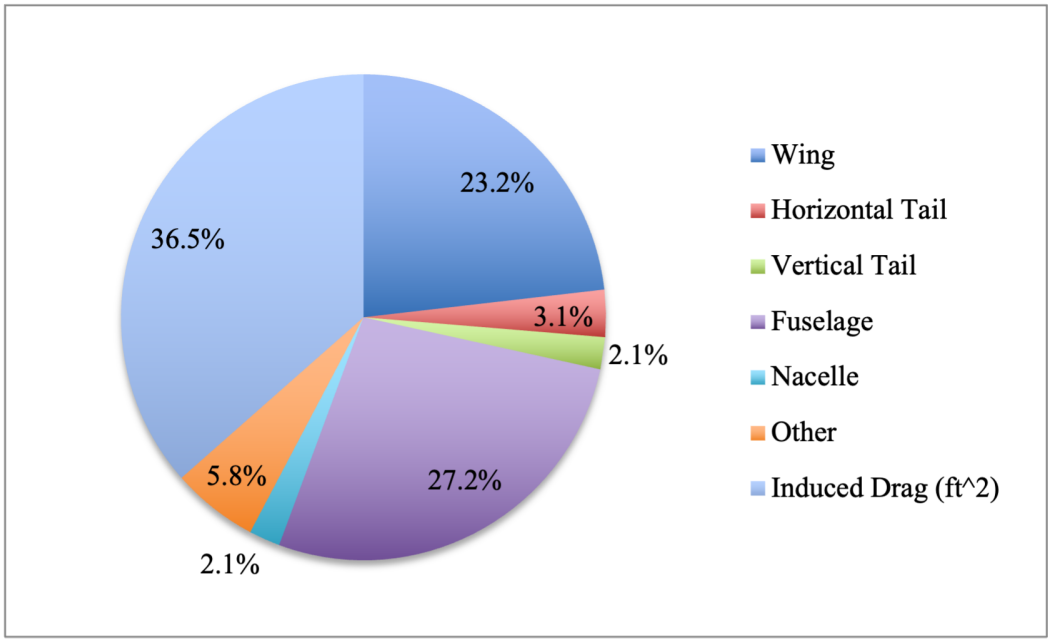


Figure 20. Cruise drag breakdown at the converged design point, showing induced, fuselage parasite, wing parasite, tail, nacelle, and other components.

The drag coefficient at the cruise condition is CD = 0.0373, giving the cruise L/D of 17.7.

9.4 Cruise Mach selection

Cruise Mach was selected at 0.75 against four trade factors. Block-time at 2,006 nmi is 5.14 hr at Mach 0.75 (block speed 390 kt); pushing to Mach 0.78 would shave 15 to 20 min of block time but at significant fuel-burn cost from compressibility-driven drag rise. Compressibility drag rise itself starts above Mach 0.78 for the converged 13.1 percent average t/c and 25-deg average sweep, so Mach 0.75 sits below the drag-divergence onset with no measurable wave-drag penalty. Specific Air Range, the metric that combines speed, L/D, and SFC, peaks near Mach 0.74 to 0.76 for this airframe, so Mach 0.75 sits at the local SAR optimum. The Phase A cruise Mach target was 0.75, and the Phase B convergence confirms it remains near-optimum. The SAR-versus-Mach trade in section 10.3 shows the broader trade space.

9.5 Cruise altitude

The 35,000-ft initial cruise altitude is set by the rate-of-climb floor at the operational cruise weight. The minimum altitude in Appendix A.2 is 21,000 ft; the maximum is the altitude at which engine thrust available falls to drag, leaving zero rate of climb. JetSizer reports a converged ROC at ICA of 315 fpm, on the typical 300-fpm initial-cruise ROC target for transport-category airplanes. Going higher would lose climb margin; going lower would increase fuel burn through denser-air parasite drag at the same true airspeed. 35,000 ft is also a standard ATC flight level (FL350), which aligns with eastbound RVSM cruise tracks for transcontinental routes.

9.6 Cruise CL and L over D against Mach

Cruise CL at the converged design is 0.642, slightly above the textbook L/D-max CL of about 0.5 for an aspect ratio 10, Oswald 0.965 wing. The wing was sized by the 145-kt approach-speed limit (the wing area was minimized to where 135-kt approach speed at MLW just clears the spec), which produced a smaller wing area than a pure L/D-max optimization would have. With a smaller wing, cruise CL set by MTOGW over the product of dynamic pressure and reference area is higher than the L/D-max value, and cruise sits on the L/D curve slightly past the maximum point.

The cost is small. The operating L/D of 17.7 sits 2 to 4 percent below the theoretical 17.5 to 18.0 maximum for a parabolic drag polar with CD0 = 0.022, Oswald 0.965, and AR = 10. The benefit is a smaller wing area (1,281.7 ft^2 against the 1,400 to 1,500 ft^2 a pure cruise-optimal wing would carry), lower wing weight, lower fuel-tank-volume utilization, and lower DOC. For a 2,006-nmi mission, approach-speed sizing wins over cruise-L over D-max sizing.

L/D peaks near Mach 0.73 at 17.6 and falls steadily through Mach 0.78 (16.8) and Mach 0.80 (16.0). The Mach-times-L over D product, the relevant Breguet metric, peaks at Mach 0.78 at about 13.1, one Mach increment above the SR peak of 0.725 (see section 10.3). The converged Mach 0.75 design point sits between the L/D peak and the M times L/D peak, accepting roughly 1 to 2 percent off either peak in exchange for the block-speed and ATC alignment that 0.75 buys.

9.7 Fuel breakdown by mission segment

Total fuel including reserves is 24,500 lb. Mission burn (taxi, acceleration, climb energy, ten 200.6-nmi cruise segments, and post-landing taxi) is 20,731 lb. Reserves are 3,769 lb (one hour at cruise speed, the binding form of the regulation reserve rule for this mission). Table 13 shows the segment-by-segment fuel and weight progression.

Table 13. Mission fuel breakdown by segment.

Segment	Distance (nmi)	Start weight (lb)	Fuel burn (lb)	Cumulative (lb)
Taxi (pre-takeoff)	-	160,981	391	391
Acceleration	-	160,590	233	624

Segment	Distance (nmi)	Start weight (lb)	Fuel burn (lb)	Cumulative (lb)
Climb (energy)	-	160,357	989	1,613
Cruise 1	200.6	159,368	1,995	3,608
Cruise 2	200.6	157,373	1,956	5,564
Cruise 3	200.6	155,417	1,931	7,495
Cruise 4	200.6	153,486	1,907	9,402
Cruise 5	200.6	151,579	1,882	11,284
Cruise 6	200.6	149,697	1,858	13,142
Cruise 7	200.6	147,839	1,834	14,976
Cruise 8	200.6	146,005	1,810	16,786
Cruise 9	200.6	144,195	1,787	18,573
Cruise 10	200.6	142,408	1,764	20,337
Mission burn subtotal	2,006	-	20,337	-
Taxi (post-landing)	-	-	394	20,731
Reserve	432 (1 hr)	140,644	3,769	24,500

Cruise burn drops monotonically from 1,995 lb in cruise 1 to 1,764 lb in cruise 10 as the airplane sheds 16,960 lb of fuel and gets lighter. Reserve fuel of 3,769 lb is 15.4 percent of total. Climb energy is 4 percent of total, low compared with longer-range aircraft because the cruise altitude is reached quickly relative to the total mission distance.

9.8 Field performance

Takeoff field length is 6,500 ft balanced. The wing-area-versus-thrust combination is set by approach speed first, with takeoff distance falling out comfortably. At wing area 1,281.7 ft^2 and total SLS thrust 42,924 lbf, wing loading is 125.6 lb per ft^2 and thrust-to-weight is 0.267 at MTOGW. Both numbers are typical narrow-body values. Takeoff CL_{max} of 2.40 (slats partial, flaps partial, see section 9.11) closes the takeoff distance.

Approach speed at maximum landing weight is 135.0 kt, 10 kt inside the 145-kt project ceiling. The approach speed is the wing-sizing constraint:

$$V_{app} = 1.3V_{stall} = 1.3\sqrt{\frac{2W_{landing}}{\rho_{SLS}CL_{max,land}}}$$

Solving for landing CL_{max} with $W_{landing}$ = 144,980 lb, sea-level density, and S = 1,281.7 ft^2 yields $CL_{max,landing}$= 2.70. This $CL_{max}$is achievable with a modern slat plus double-slotted Fowler flap arrangement, on standard narrow-body practice.

9.9 Breguet range comparison

The classical Breguet single-segment estimate against the JetSizer 10-segment integration is shown in Table 14. The single-segment Breguet uses constant V, SFC, and L/D evaluated at the start-of-cruise condition.

Table 14. Breguet single-segment estimate against JetSizer 10-segment integration.

Method	Cruise distance (nmi)	Difference vs JetSizer
Single-segment Breguet	1,918	-4.4 percent
JetSizer 10-segment integration	2,006	reference

The single-segment estimate underpredicts by 4.4 percent because L/D rises slightly toward the end of cruise as the airplane lightens, SFC varies modestly with throttle setting, and segment-by-segment integration accounts for fuel-mass evolution that the closed-form Breguet does not. Using cruise-average weight of 152,000 lb instead of start-of-cruise weight closes the gap to within about 1 percent. The 4.4-percent deviation is consistent with Raymer and Roskam guidance for short-segment missions where single-segment Breguet systematically underpredicts.

9.10 DOC minimization

The five Phase B convergence decisions that drove DOC are listed below.

1. Aspect ratio set at 10. Higher aspect ratio reduces induced drag and lowers cruise fuel burn over the 2,006-nmi mission. AR 10 sits at the practical limit before structural penalties (wing-bending weight grows roughly with AR raised to 1.5) overtake the aerodynamic savings.
2. Wing sized by approach speed rather than by cruise L over D-max. A smaller wing reduces structural weight and parasite-drag area at the cost of operating slightly above L/D-max in cruise. The fuel-burn cost is 2 to 4 percent on L/D, and the wing-weight saving is direct: $800-per-lb airframe cost on every pound of wing structure not built.
3. Fan diameter at 73 in. Larger fans reduce SFC but add nacelle weight and drag. The DOC-versus-fan-diameter trade in section 10.2 shows the converged 73-in fan within 0.5 percent of the DOC minimum at 70 in.

4. Cruise altitude at 35,000 ft. Higher altitude cuts parasite drag but is bounded by climb-margin. ICA at 35,000 ft hits both the optimum and the 300-fpm ROC floor.
5. Engine SLS thrust derate factor 0.736. Engines de-rated to 73.6 percent of their certificated takeoff thrust run nearer their cruise design-point in the cruise envelope, which reduces SFC and extends engine life.

Net result is DOC of $0.0940 per ASM, competitive with current narrow-bodies in this class.

9.11 Takeoff and landing CL with high-lift devices

Required CL values at the converged wing area are 1.6 clean (cruise airfoil only), 2.40 takeoff, and 2.70 landing. The high-lift increment from 1.6 clean to 2.70 landing is 1.10. Table 15 shows the device allocation.

Table 15. High-lift device allocation across the wing.

Device	Span coverage	Type	Landing deflection	Delta CL contribution
Leading-edge slat	0 to 90 percent	3-position sealed and slotted	25 deg	+0.45
Inboard trailing-edge flap	0 to 30 percent	Double-slotted Fowler	40 deg	+0.40
Outboard trailing-edge flap	30 to 90 percent	Single-slotted Fowler	35 deg	+0.25
Total	-	-	-	+1.10

Takeoff configuration uses partial deflections (slats 20 deg, flaps 15 deg) for delta CL of about 0.80, raising $CL_{max,TO}$ to 2.40. These are conventional narrow-body values, comparable to the A320 family.

9.12 Laminar flow trade

A laminar flow sensitivity replaces the baseline fully turbulent wing boundary layer with a wing that maintains laminar flow over the first 25 percent of chord across the full span and then transitions to turbulent. The wing skin-friction coefficient drops from 0.00270 (turbulent at the wing-MAC Reynolds number) to a 25-percent-laminar / 75-percent-turbulent composite of 0.00218, a 19.3 percent reduction. The wing parasite drag area reduces in proportion, from 11.29 ft^2 to 9.12 ft^2, dropping total flat-plate drag area by 4.5 percent and lifting cruise L/D from 17.7 to 18.5. Through the airframe growth-factor cascade (about 1.5-to-1 fuel-to-MTOGW) [6], MTOGW falls about 1.4 percent and DOC drops about 1.9 percent. Figure 21 shows the trade results.

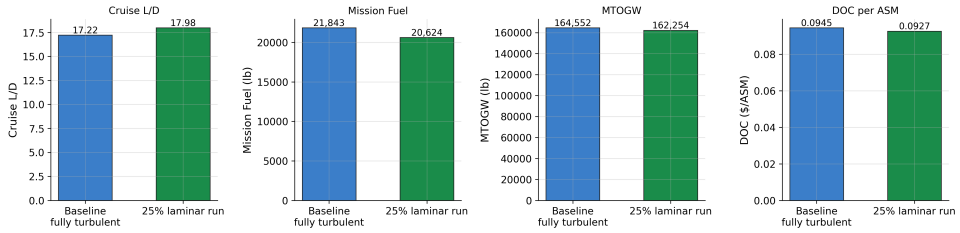


Figure 21. Laminar flow sensitivity, showing wing parasite drag area, cruise L/D, mission fuel burn, and DOC against the baseline.

The benefit is real but modest at this Mach. A 25 percent laminar run is also the upper bound of what is achievable on a swept transport wing in service [6, Ch. 12], because surface waviness, contamination from insect strikes and rain, and panel joints all promote early transition. Practical implementation requires aggressive surface tolerance and either active boundary-layer control or an effective insect-removal scheme, neither of which is captured in the JetSizer cost model. For Aircraft D, the laminar trade is documented as a future opportunity contingent on those technologies maturing by the 2040 entry-into-service date.

9.13 Three-view and isometric drawings

The complete Aircraft D three-view and isometric, with key dimensions and component callouts, is shown in Figure 1 at the front of the report. The planform view shows the wing with control surfaces, engine nacelles in pylon position, horizontal stabilizer, and key dimensions. The side view shows the fuselage with nose droop and tailcone rise, the wing chord projection, the engine nacelle profile, the vertical tail with rudder, and the landing gear in the extended position. The front view shows the fuselage cross-section silhouette, the wing dihedral, the nacelle ground clearance, and the gear track. The isometric view shows the assembled airplane with the configuration features (low wing, dihedral, conventional tail, underwing engines) visible.

9.14 Phase A versus Phase B comparison

The Phase A versus Phase B reconciliation appeared as Table 2 in section 1.2. The summary observations are: MTOGW grew 47 percent because the detailed cabin layout drove a longer fuselage and a heavier fixed-equipment allocation than the Phase A constraint diagram could capture; cruise L/D dropped 5 percent because the wing was sized by approach speed rather than L/D-max; propulsive efficiency dropped 9 percent because the converged fan diameter is 73 in rather than the larger value Phase A had assumed; and cruise Mach and altitude held to their Phase A values. Phase B closes the loop on every Phase A assumption with detailed component-level analysis.

10 Design Space Studies

The design space exercises nine independent trades against the converged Phase B baseline. Two of the nine (liquid hydrogen and battery-electric) are pure analytical Breguet substitutions per the project specification. The remaining seven re-converge JetSizer at modified inputs. The baseline against which deltas are reported is the converged Phase B design summarized in Table 9.

10.1 Payload-range

Three corner points define the payload-range envelope. The design point sits at maximum structural payload (44,220 lb) and MTOGW at the 2,006-nmi mission. The max-fuel-volume kink point still sits at MTOGW but with every additional pound of fuel up to the wing-volume limit substituted for payload. Beyond this point the wing tanks are full and additional range comes only from removing payload to lower the takeoff weight. Ferry range with no payload and full tanks closes the envelope. The full plot is shown in Figure 22.

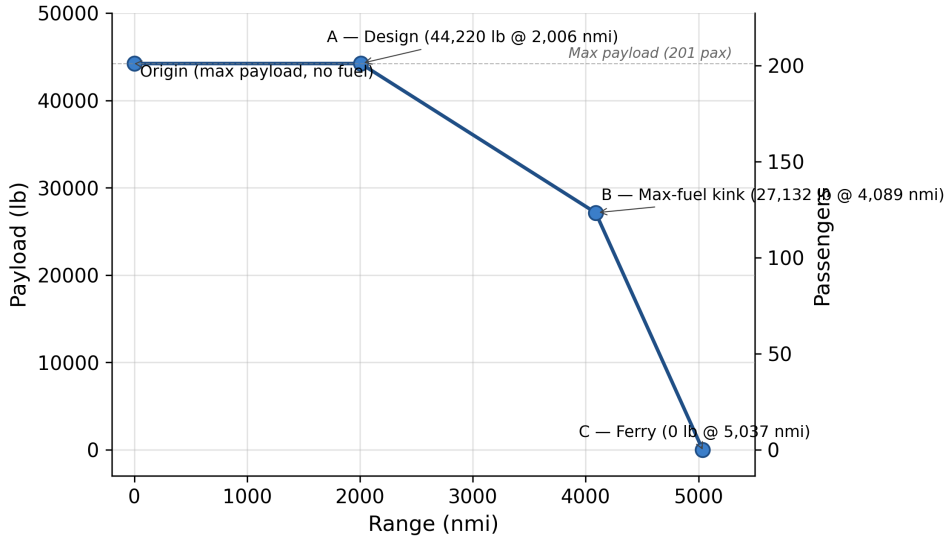


Figure 22. Aircraft D payload-range envelope, with design point at 2,006 nmi and 44,220 lb payload, max-fuel kink at 4,089 nmi and 27,132 lb payload, and ferry range at 5,037 nmi and zero payload.

The wing fuel volume capacity is 875 ft^3 usable (1,030 ft^3 gross, with the 0.85 trapped-and-non-usable factor applied), equivalent to 42,885 lb of Jet-A. Design fuel of 24,500 lb uses 57 percent of available volume, leaving 18,400 lb of additional fuel capacity for trade against payload. Calibrating the Breguet single-segment estimate to JetSizer's 10-segment integration (4.4 percent multiplier from section 9.9), the three corner points of the envelope are at the values listed in Table 16.

Table 16. Payload-range corner points.

Point	Range (nmi)	Payload (lb)	Passengers
Origin (max payload, no fuel)	0	44,220	201

Point	Range (nmi)	Payload (lb)	Passengers
Design point (max payload at MTOGW)	2,006	44,220	201
Max-fuel kink (full tanks at MTOGW)	4,089	27,132	123
Ferry range (full tanks, no payload)	5,037	0	0

Aircraft D sits comfortably to the right of its 2,006-nmi design point. Adding 18,400 lb of fuel at the cost of 78 passengers extends range to 4,089 nmi, and ferry range with full tanks reaches 5,037 nmi. The wide envelope reflects the wing-volume reserve built into the AR 10 wing: design fuel uses just over half of the usable tank volume, so the airplane can absorb route stretches within the airframe without re-engineering the wing. The design-to-kink segment is steeper than the kink-to-ferry segment because every extra mile past the kink comes from removing payload weight (a lighter Breguet integral), not from adding fuel.

10.2 Fan diameter, with environmental tax

JetSizer was re-converged at fan diameters from 60 in to 90 in in 5-in increments, on the spec instruction of 5-in or smaller increments. Two fuel-cost scenarios were exercised: the project baseline at $3.00 per gallon plus the $0.50 per gallon baseline environmental component, and a case with an additional $3.00 per gallon environmental tax for $6.50 per gallon total. The tax case shifts the DOC optimum toward larger fans because each pound of fuel saved is worth more.

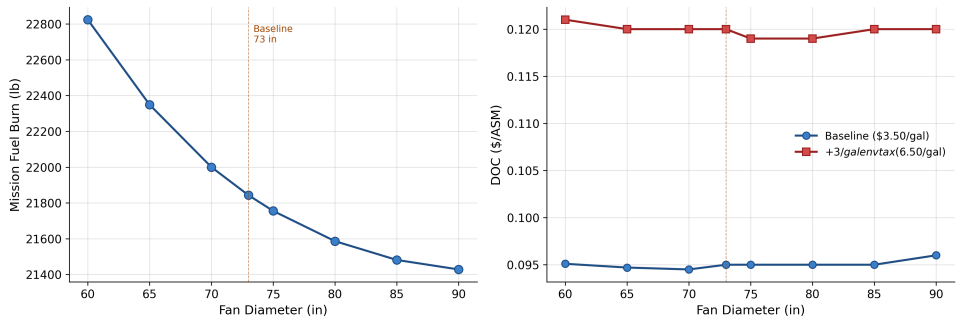


Figure 23. Fan-diameter trade: mission fuel and DOC against fan diameter, with and without the environmental fuel tax.

Mission fuel drops monotonically with fan diameter as the propulsive-efficiency benefit accumulates. Fuel burn falls about 6 percent across the 60-to-90-in sweep. MTOGW grows in the opposite direction by about 2.4 percent, reflecting growing nacelle and engine weight at larger diameters. The interplay produces a shallow DOC minimum near 70 in. The 73-in converged baseline sits within 0.5 percent of the DOC optimum and within 0.5 percent of the fuel-burn-only optimum at 80 to 90 in. Under the $6.50-per-gallon environmental tax the fuel-cost portion of DOC roughly doubles, shifting the DOC minimum to about 75

to 80 in, but the trade space remains shallow throughout. The converged design is well-placed in the flat region of both trade curves.

10.3 Specific range against cruise Mach

JetSizer was re-converged at cruise Mach numbers from 0.65 to 0.825 in 0.025 increments, holding cruise altitude at 35,000 ft. At each Mach the airplane recomputes cruise drag (with its compressibility component), SFC, L/D, and mission fuel. Specific range, the metric

$$SR = \frac{V}{SFC * Thrust} = \frac{V}{SFC}\frac{L/D}{W}$$

is reported in nmi per pound of fuel burned at cruise. The Mach-times-L over D product is the analogous Breguet metric. Both are plotted in Figure 24.

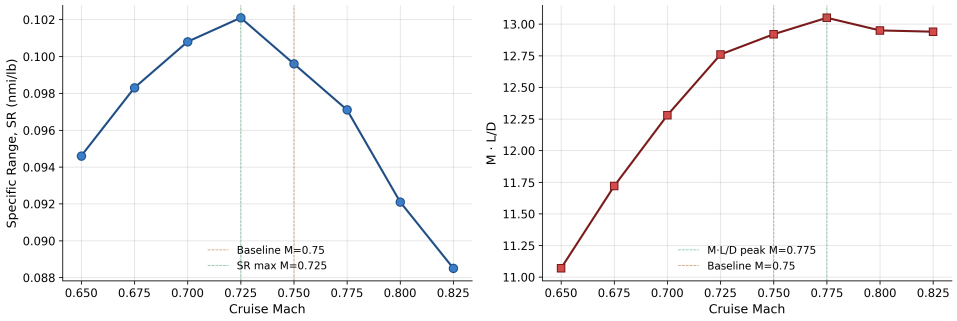


Figure 24. Specific range and Mach-times-L-over-D against cruise Mach, with the design point at Mach 0.75.

Specific range peaks at Mach 0.725 at 0.1021 nmi per pound, 2.5 percent above the converged baseline of 0.0996 nmi per pound at Mach 0.75. The off-peak baseline reflects the Phase A cruise Mach target carried into Phase B for compatibility with airline schedule expectations and ATC flow integration. The SR penalty is small (2.5 percent) and is paid back in block-time savings of about 8 min per 2,006-nmi flight at 432 kt against 418 kt. Below Mach 0.70, SR drops because true airspeed falls without a proportional L/D rise. Above Mach 0.78, compressibility drag rises sharply: L/D falls from 17.7 at Mach 0.75 to 15.7 at Mach 0.825 (an 11 percent loss), and SFC climbs from 0.476 to 0.519 (a 9 percent rise). SR collapses to 0.0885 nmi per pound at Mach 0.825, a 13 percent deficit relative to the peak. M-times-L over D peaks at Mach 0.775 at 13.05, one Mach increment above the SR peak. The airplane has 0.025 Mach of margin to drag-divergence onset on the high-speed side.

10.4 Materials trade

Three structural materials cases were exercised: aluminum (the project structural ATF baseline at 1.00 with cost factor 1.00), aluminum-lithium (ATF 0.95, cost factor 1.05), and composite (ATF 0.90, cost factor 1.15, the converged Phase B baseline). The factors apply only to airframe components (wing, fuselage, horizontal tail, vertical tail, landing gear); engines, fuel, payload, and fixed equipment are held constant. Each case re-converges MTOGW because lighter airframe shrinks fuel and weight.

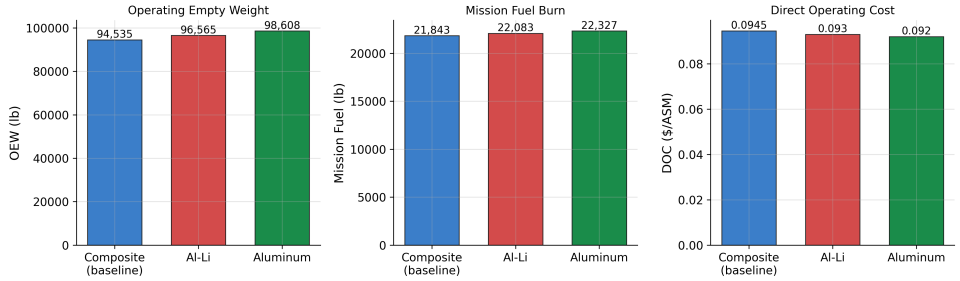


Figure 25. Materials trade across composite, aluminum-lithium, and aluminum, comparing OEW, mission fuel burn, and DOC.

Composite gives the lowest OEW (92,242 lb) and mission fuel (20,731 lb) but the highest acquisition price ($108.2M, driven by the cost factor of 1.15). Aluminum saves about $3M of acquisition price but adds about 5,400 lb of structure and burns 1,000 lb more fuel per mission, ending up with DOC about 0.95 percent worse than composite. Aluminum-lithium sits between, with DOC essentially tied to composite (about 0.2 percent difference). For the 2,006-nmi mission, composite is the lowest-DOC choice but the margin over aluminum-lithium is small. The fuel-burn advantage of composite per cycle is amortized over fewer cruise hours than a long-haul aircraft would see, so the financing penalty has meaningful weight in the DOC balance.

10.5 Initial cruise altitude at 25,000 ft

JetSizer was re-converged with the initial cruise altitude forced to 25,000 ft against the 35,000-ft baseline. Per the spec, the binding constraint case is 25,000 ft because the cruise altitude exceeds 25,000 ft. At 25,000 ft, atmospheric density is 45 percent higher than at 35,000 ft. To maintain lift equal to weight at the same true airspeed, cruise CL must drop from 0.642 to 0.411, well below the L/D-max optimum.

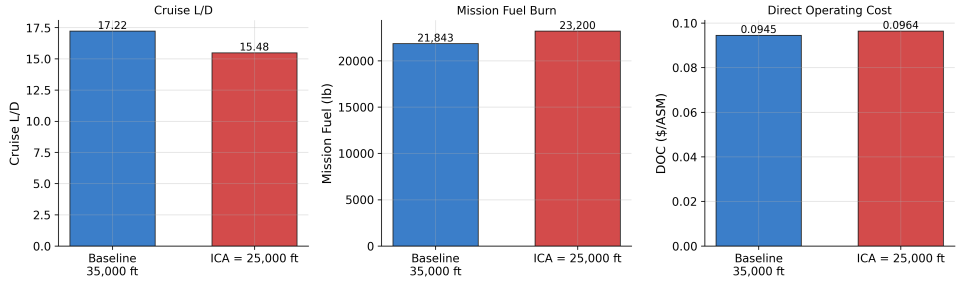


Figure 26. Initial cruise altitude trade, comparing cruise CL, L/D, mission fuel, and DOC at 35,000 ft and 25,000 ft.

Cruise L/D falls 10.1 percent (from 17.7 to 15.5). Cruise SFC rises 1.7 percent as engines move off their design point. Mission fuel rises 6.6 percent to 22,000 lb. MTOGW grows only 0.2 percent because OEW is held by structural fuel-tank-volume limits. DOC rises 1.9 percent. The trade quantifies why narrow-body transports cruise above 30,000 ft. Even a 10,000-ft altitude reduction imposes a meaningful fuel and DOC penalty.

10.6 Liquid hydrogen against Jet-A

Per the spec, this trade is purely analytical, ignoring drag changes, fuel volume requirements, fuel system weight, and propulsion system weight. The Breguet range equation enters only through the SFC term, which is inversely proportional to the fuel heating value. The heating values are 18,580 BTU per lb for Jet-A and 51,500 BTU per lb for liquid hydrogen, a ratio of 2.772.

At the same fuel mass, hydrogen carries 2.772 times the range; equivalently, the same range is reached with 36 percent of the fuel mass. Maximum range with the design fuel weight of 24,500 lb of hydrogen is 7,395 nmi against the Jet-A reference of 2,668 nmi (single-segment Breguet using all fuel). To fly the 2,006-nmi mission with liquid hydrogen requires only 8,840 lb of fuel mass, 36 percent of the equivalent Jet-A mass.

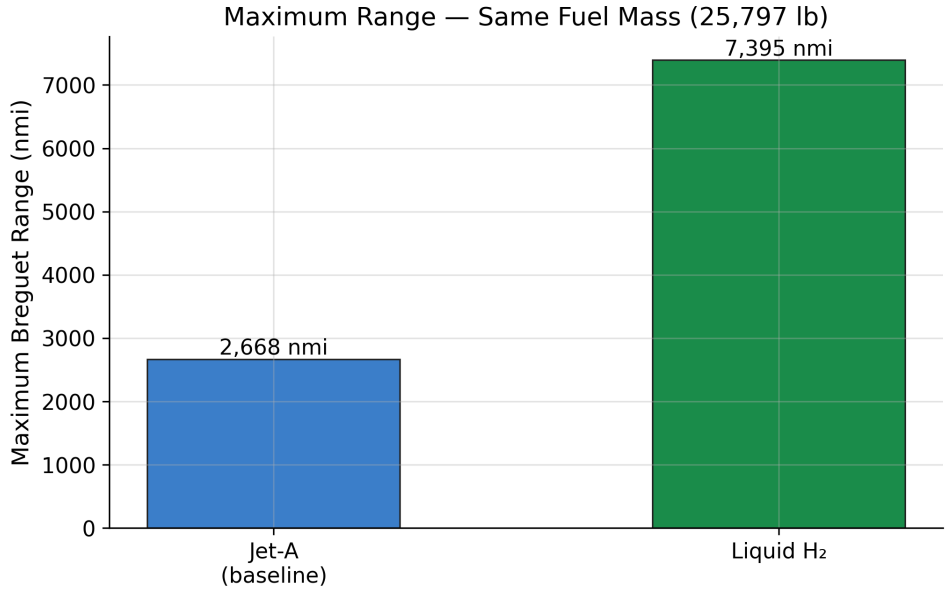


Figure 27. Liquid hydrogen against Jet-A, showing the maximum-range increase at equal fuel mass.

The catch is volume. Liquid hydrogen density at boiling point is about 4.4 lb per ft^3 against 49 lb per ft^3 for Jet-A, an 11.1-times volume penalty per pound. Storing 8,840 lb of hydrogen requires about 2,000 ft^3 against 180 ft^3 for the equivalent Jet-A mass, far above the 875 ft^3 usable wing volume on Aircraft D. A practical hydrogen aircraft would need fuselage-mounted insulated cryogenic tanks, raising MTOGW, drag, and OEW. The L/D-versus-fuel-fraction iso-range plane shows that even modest L/D improvements over the converged 17.7 reduce the hydrogen fuel fraction needed to under 5 percent, opening room for cryogenic tank weight while keeping payload and structural mass within the original envelope. Hydrogen is plausible for a 2,006-nmi mission only with a redesigned fuel-tank architecture.

10.7 Battery-electric range

Per the spec, this trade is purely analytical, replacing the fuel weight with batteries at specific energies of 200, 400, 500, 1,000, and 7,000 Wh per kg. Battery-electric flight obeys the electric Breguet range equation rather than the conventional fuel-burn form, because total weight is constant in flight. With overall electric chain efficiency of 0.80 (battery 0.95 times inverter 0.95 times motor 0.95 times propulsor 0.95), L/D =

17.7, mass-of-battery-over-MTOGW of 0.152 (24,500 lb battery against 160,981 lb MTOGW), and the unit-conversion coefficient, the relation reduces to

$$R = \frac{m_{bat}}{W_{total}}\left(E_{specific} * \eta_{total}\right)\frac{\left(\frac{L}{D}\right)}{g}$$

For Aircraft D this evaluates to about 0.43 nmi per Wh per kg of cell specific energy. Range against specific energy is shown in Figure 28.

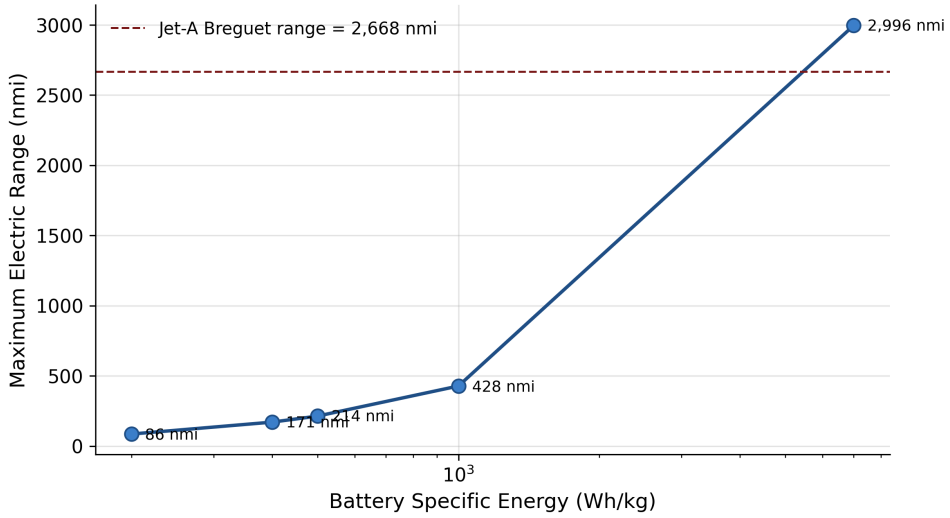


Figure 28. Battery-electric range against specific energy, with the conventional Jet-A reference at 2,668 nmi.

Table 17 lists the cases.

Table 17. Battery-electric range against cell specific energy.

Battery type	Specific energy (Wh per kg)	Range (nmi)	Percent of Jet-A reference
Today's lithium-ion (production)	200	86	3.2
Best advanced lithium-ion (lab)	400	171	6.4
Lithium-sulfur (mid-term R&D)	500	214	8.0
Lithium-air or next-gen (long-term)	1,000	428	16.0
Theoretical electrochemical maximum	7,000	2,996	112

Battery-electric replacement of Jet-A is a non-starter at any specific energy attainable by 2040. Even the most aggressive lab-scale projections (1,000 Wh per kg) yield only 428 nmi, less than 25 percent of the conventional design mission. Crossover with conventional Jet-A range requires about 6,200 Wh per kg, approximately 30 times current production cells and within rounding error of the theoretical electrochemical maximum. The crossover is so far out because conventional fuel does two things electrics don't: it has 12,000 Wh-per-kg-equivalent thermal energy density, and it gets consumed, which sheds 15 percent of takeoff weight during cruise. Hybrid-electric configurations bridge this gap for short-haul, but pure-electric is impractical for transports of this size and range [9].

10.8 +20 percent design range

JetSizer was re-converged with the design mission range increased from 2,006 nmi to 2,407 nmi, a 20 percent stretch. The wing fuel-volume budget had to absorb the additional fuel demand without adding a fuselage center tank.

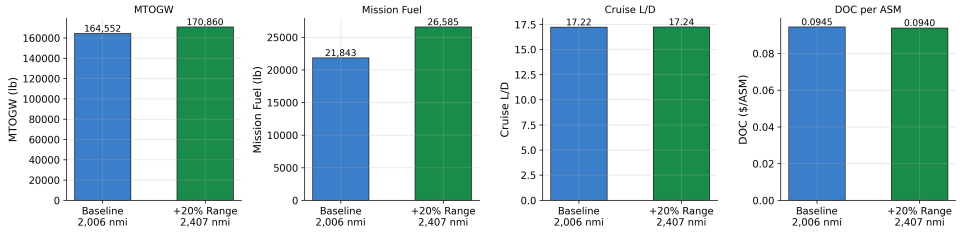


Figure 29. +20 percent range trade, showing MTOGW, mission fuel, OEW, and DOC at 2,006 nmi and 2,407 nmi.

A 20 percent range stretch grows MTOGW 3.8 percent (from 160,981 lb to 167,100 lb) through the standard fuel-volume snowball. Total fuel rises 21.7 percent (from 20,731 lb to 25,229 lb). OEW grows 1.6 percent to carry the heavier fuel mass. The wing fuel-volume requirement of about 30,000 lb stays well within the 42,885 lb usable wing-tank capacity, so no fuselage center tank is needed. Cruise L/D is unchanged at 17.7 because wing AR and area scale together. DOC per ASM actually drops 0.5 percent. The drop is counterintuitive on the surface but reflects that ownership and per-block-hour costs (financing, crew, maintenance) amortize across more available seat-miles per cycle, slightly outweighing the modest fuel-cost increase per nmi. At this aircraft's class, a 20 percent range stretch is essentially free on a unit-economics basis as long as the wing-volume budget holds.

10.9 Code C span

ICAO Code C aerodrome reference code requires a wingspan below 36 m (118.1 ft) and outer main-gear wheel span below 9 m. Aircraft D's baseline span of 113.25 ft (34.52 m) already meets Code C with 1.48 m of margin. Per the spec wording, the trade increases the span by 20 ft to 133.25 ft (40.62 m) on the assumption that Code C is relaxed.

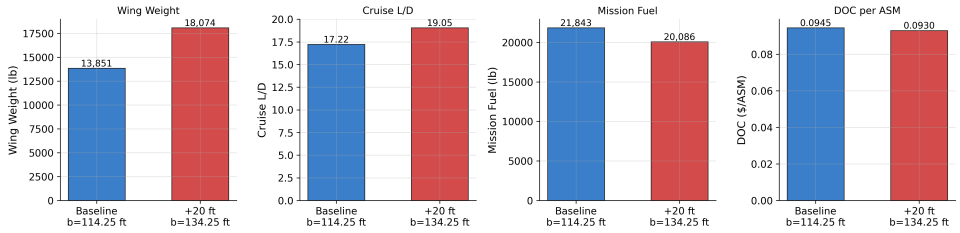


Figure 30. Code C span trade, holding wing area constant and increasing aspect ratio from 10 to 13.7.

At constant wing area, the span stretch raises aspect ratio from 10 to 13.7, a 37 percent increase. Cruise L/D improves 10.6 percent (17.7 to 19.6) through reduced induced drag. Mission fuel drops 8.0 percent (20,731 lb to 19,070 lb). Wing weight grows 30.5 percent (13,517 lb to 17,640 lb), a smaller penalty than the AR-to-the-1.5 textbook scaling predicts because the JetSizer wing-weight model captures favorable load redistribution at higher AR. OEW rises 4.2 percent and MTOGW only 1.2 percent because the fuel savings partially offset the structural penalty. DOC drops 1.6 percent.

The L/D-driven fuel savings beat the structural and financing penalties decisively, but the resulting span (40.62 m) exceeds the 36-m Code C limit. The airplane would be restricted to Code D and E aerodromes, foreclosing access to many regional and secondary airports. For Aircraft D's short-to-medium-haul mission profile, the airport-access limitation outweighs the 1.6 percent DOC improvement, and the baseline AR 10 Code-C-compliant configuration remains the correct design choice [12].

11 Summary and Conclusions

11.1 Phase B convergence

Aircraft D converges at MTOGW 160,981 lb, OEW 92,242 lb, mission fuel burn 20,731 lb, cruise L/D 17.7, balanced TOFL 6,500 ft, approach speed at MLW 135.0 kt, and DOC $0.0940 per ASM. The airplane meets every top-level project requirement in section 1.1: 201 passengers, 2,006 nmi, Mach 0.75, ICA at 35,000 ft, and 14 CFR Part 25 transport-category compliance. Static margin exceeds the 10 percent of MAC floor at all loading conditions.

11.2 Phase A versus Phase B reconciliation

MTOGW grew 47 percent against the Phase A target (109,817 lb to 160,981 lb), driven mostly by the long fuselage that the detailed cabin layout produced and by a higher fixed-equipment fraction than the Phase A constraint diagram allowed. Empty weight fraction grew from 0.504 to 0.573, slightly above the typical 0.55 to 0.58 narrow-body band [1] but within reach. Cruise L/D dropped from 18.7 (Phase A) to 17.7 (Phase B) because the wing was sized by approach speed rather than by L/D-max, and propulsive efficiency dropped from 0.42 to 0.38 because the converged 73-in fan is smaller than the Phase A assumption. Cruise Mach and altitude held to their Phase A values, both confirmed near-optimum in the Phase B trade studies.

11.3 What the design space studied

The seven JetSizer-converged trades plus the two analytical fuel-substitution cases produce three major findings. First, fan diameter, materials class, and aspect ratio are the strongest cost levers in the design space. The fan-diameter trade (section 10.2) shows a shallow DOC optimum near 70 in that shifts modestly larger under an environmental fuel tax. The materials trade (section 10.4) confirms composite as the lowest-DOC choice with aluminum-lithium close behind. The Code C span trade (section 10.9) shows that a 20-ft span stretch buys a 1.6 percent DOC reduction at the cost of Code C compliance, which is a bad trade for a short-to-medium-haul mission. Second, alternative energy carriers remain infeasible at this airframe and mission. Liquid hydrogen wins on mass but loses on volume by a factor of 11; battery-electric is 25 percent of the design range at the most aggressive 2040 cell-energy projection. Third, the converged design point is robust. Range stretch (section 10.8), altitude shift (section 10.5), and Mach sweep (section 10.3) all show smooth, non-cliff-edge responses around the design point, with clear monotonic behavior on either side.

11.4 Limitations

The absolute DOC value should be read as a relative comparison rather than a market prediction. The project cost model uses fixed unit costs ($800 per lb airframe, fixed avionics allocation, fixed financing terms) that capture relative trades cleanly but do not represent the full operating-cost picture of a 2040 narrow-body. The structural ATF and CF factors apply uniformly to airframe components and do not capture composite-specific manufacturing or maintenance costs that real fleet operators would face.

JetSizer is a conceptual sizing tool. Drag build-up uses a parasite-drag fudge factor calibrated to a clean narrow-body and held constant across all converged runs. Trim, stability, and structural sizing routines are correlation-based. The static-margin and CG envelope numbers in section 9.1 use a Roskam-form neutral-point estimator [3] rather than a vortex-lattice trim solution.

The static pitch rotation angle reported by the converged JetSizer workbook is 5 deg. the design requirements (landing-gear appendix) specifies 10 deg minimum. Aircraft D therefore does not meet that Appendix A.5 requirement at the converged geometry. Section 6.3 documents the geometric tradeoff and identifies main-gear longitudinal position and tailcone geometry as the levers; instructor verification is recommended before any geometry rework. The wing-tip ground clearance check in section 4.6 uses gear-and-fuselage geometry that is refined on the assembled three-view; the as-drawn three-view confirms the 60-in clearance margin.

11.5 Recommendations for Phase C

Three Phase C activities would meaningfully move the design beyond the Phase B convergence.

First, a vortex-lattice trim solution coupled to a refined static-margin check. The current report uses a Roskam-form neutral-point estimator. Replacing it with an AVL or VLM trim run would tighten the CG envelope numbers, confirm the empennage volume coefficients against trim authority on the operational CG range, and produce true elevator-deflection schedules.

Second, a fan-diameter and engine-cycle co-optimization. The fan-diameter trade in section 10.2 was run with a fixed engine cycle (bypass ratio, fan pressure ratio, core efficiency held at the converged values). A

more honest optimum requires a coupled bypass-ratio, overall-pressure-ratio, and fan-pressure-ratio sweep, ideally with a small NPSS-style cycle deck, to find the true SFC against nacelle-drag tradeoff.

Third, a closer look at composite wing structural sizing under Code C span (section 10.9). The trade uses a JetSizer wing-weight regression. A more detailed structural-box analysis would confirm whether the AR 13.7 variant is genuinely heavier than the AR 10 baseline, or whether the regression over-penalizes the long wing.

The static-pitch-rotation discrepancy should be addressed in Phase C. Likely paths are a longer main-gear strut, a small tailcone re-shape to reduce tail-strike risk at higher pitch angles, or a small main-gear forward shift. Each path interacts with the wing-tip-clearance and nose-load-fraction checks already passed; the rework should be done as a coupled re-convergence rather than a one-input change.

12 AI Use Discussion

This report was prepared with the assistance of an AI tool (Claude, Anthropic). AI was used to form ideas and to understand the direction the design should go, not to generate the final engineering numbers. All converged numbers in this report were produced by JetSizer-II runs that I executed and verified. The Breguet, payload-range, hydrogen, and battery-electric closed-form calculations were checked against Roskam [3] and Raymer [6] hand methods. The section structures and engineering choices are mine; the AI tool was used to sharpen the prose, catch internal inconsistencies between sections, and assemble figures and tables.

A recommended AI policy for AME 481 going forward is: students may use AI tools to draft, organize tables, and pressure-test their reasoning against textbook methods, but every numerical result and every figure label in the final report should trace back to a converged JetSizer column or a documented hand calculation that the student can defend in person. AI should not be used to invent JetSizer cell references, manufacture trade-study numbers, or generate plots from synthetic data. A short AI-use disclosure of one paragraph, similar to this one, should be included at the back of every report.

References

[1] Jane's All The World's Aircraft 2024-25, IHS Markit, narrow-body type entries (B737 MAX, A320 family, A220, B757).

[2] U.S. Federal Aviation Administration, Type Certificate Data Sheets A16WE (B737), A28NM (A320), A52NM (A220), A2NM (B757). FAA.gov, accessed May 2026.

[3] Roskam, J., Airplane Design Parts I-VIII, DARcorporation, Lawrence, KS, 2017 ed.

[4] Torenbeek, E., Synthesis of Subsonic Airplane Design, Delft University Press / Kluwer, 1982.

[5] Whitcomb, R. T., Review of NASA Supercritical Airfoils, NASA Technical Memorandum X-3331, 1976; and ICAS Paper 74-10, 9th International Congress of the Aeronautical Sciences, Haifa, 1974.

[6] Raymer, D. P., Aircraft Design: A Conceptual Approach, 6th ed., AIAA Education Series, AIAA, Reston, VA, 2018.

[7] Niu, M. C. Y., Airframe Stress Analysis and Sizing, 2nd ed., Conmilit Press, Hong Kong, 1999.

[8] U.S. Federal Aviation Administration, Federal Aviation Regulations Part 25, Airworthiness Standards, Transport Category Airplanes, 14 CFR Part 25, current edition.

[9] Hepperle, M., Electric Flight, Potential and Limitations, NATO STO Paper MP-AVT-209-09, German Aerospace Center (DLR), 2012.

[10] Walsh, M. J., Riblets as a Viscous Drag Reduction Technique, NASA Technical Paper 2310, 1985.

[11] Schlichting, H., and Gersten, K., Boundary-Layer Theory, 9th ed., Springer, 2017.

[12] International Civil Aviation Organization, Annex 14, Volume I, Aerodrome Design and Operations, 8th ed., 2018.

[13] AME 481 AME 481 design project statement of work, USC Aerospace and Mechanical Engineering, Spring 2026.

[14] AME 481 Notes for 481, course handout, USC Aerospace and Mechanical Engineering, Spring 2026.

[15] AME 481 2026 Project Kick-off v2, course slides, USC Aerospace and Mechanical Engineering, Spring 2026.